



African Journal of Biological Sciences

Journal homepage: <http://www.afjbs.com>

Research Paper

Open Access

Research article

FORMULATION, EVALUATION & *IN-VIVO* STUDY OF TOPICAL EMUL GEL LOADED WITH SILVER SULFADIAZINE FOR WOUND HEALINGAnkit Kumar¹, Manish Pathak^{1*}¹Faculty of Pharmacy, Swami Vivekanand Subharti University, Meerut (U.P) INDIA-250005

* Corresponding author

Dr. Manish Pathak

Associate Professor Faculty of Pharmacy Swami Vivekanand Subharti University, Meerut,
(U.P) INDIA-250005

e-mail:manishpharm01@gmail.com

Contact no: +91-9125532749

Article History

Volume 6, Issue 9, 2024

Received: 17 Apr 2024

Accepted : 06 May 2024

doi: 10.33472/AFJBS.6.9.2024.3320-3366

ABSTRACT

Objective: The current work aimed to create and analyze an emulgel based on nanosponges loaded with silver sulphadiazine for topical administration in wound healing, using the emulsion solvent diffusion method.

Methods: Using ethyl cellulose, xanthan gum, and polyvinyl alcohol in various drug-polymer ratios, an emulsion solvent diffusion approach was used to create the silver sulphadiazine nanosponge. Fourier transform infrared spectroscopy (FTIR) and differential scanning calorimetry (DSC) were used to determine the compatibility of silver sulphadiazine with polymer. Every formulation was assessed using entrapment efficiency, drug loading, scanning electron microscopy (SEM), transmission electron microscopy, zeta potential, in-vitro drug release, stability tests, and scanning electron microscopy.

Results: There was no interaction between the medication and the polymer, according to the DSC and FTIR studies. Melting point of silver sulphadiazine is between 253°C and 255°C. It is a white powder with no smell. A straight-line curve with an R² value of 0.9992 is produced by the calibration curve of silver sulfadiazine in a 0.5M NaOH solution. The PDI varied from 0.153 to 1.000, whereas the particle size varied from 132 to 782.4 d. nm. Value of zeta potential between -14.8 and 53.04 mV. The silver sulfadiazine DSC curve exhibits a distinct exothermic peak at 261.34°C, signifying its microcrystalline structure. The optimal formulation's entrapment efficiency and drug content were determined to be 92.49±0.88, 91.49±0.88, 92.90, and 95.26. It was discovered that the silver sulphadiazine particles were spherical in shape and ranged in size from 10 to 60 nm. The medication was discovered to be trapped over the Silver sulphadiazine, which is represented by the structures' black sections. Following the encapsulation of the silver sulphadiazine drug inside the nanosponge, the size and form stayed the same in SEM. The method utilized to construct burn wounds consistently produced partial thickness burn lesions, according to a histological analysis of the stained samples.

Conclusion: The outcomes gathered from various assessment criteria showed that the topical application of an emulgel based on silver sulphadiazine nanosponges for wound healing is a novel and successful strategy.

Keywords: Nanosponge, Emulsion solvent diffusion method, Silver sulfadiazine

1. INTRODUCTION

Burn wounds have been among the most devastating form of injuries during the last decades. Serious thermal injuries cause high mortality and morbidity. Burn patients are very prone to infections due to the loss of their natural barrier, prolonged hospital stays and therapeutic and diagnostic procedures **Oncul et al., 2002**. Previous research has demonstrated that a variety of bacterial species can easily infect burn wounds. The most prevalent species have been determined to be *S. aureus* and *P. aeruginosa*. It's interesting to note that following the initial infection, changes occur in the variance of bacterial flora and the colonization rate over time **Taneja et al., 2013**. The human skin is an important barrier to the external environment. It is responsible for immunologic protection, thermoregulation and control of fluid levels. Thereby, the natural colonization of microorganisms on the human skin also offers protection against pathogenic microorganisms by bacterial interference **Kong et al., 2011**. Serious thermal injury may cause disruption in certain physiological functions of the skin. This can result in several harmful conditions such as reduced immunity, infection, scarring and fluid loss as well **Wysocki et al., 2002**. Burn injuries cause breaches in the skin by destroying its cellular compounds. The amount of cellular damage varies based on the range of the heat that the skin was exposed to. Thermal burns denature proteins, destroy cell membranes and release oxygen-free radicals. Three different zones can be distinguished within burn wounds.

- a) Dead tissue (zone of coagulation)
- b) Viable tissue, which is at risk for ongoing damage (zone of stasis)
- c) Normal skin with minimal injury, which still shows blood flow (zone of hyperaemia)

Jackson et al., 1953.

Furthermore, local and systemic inflammatory responses are also initiated after a burn, which has detrimental effects on both the burn wound and several distant organ systems. The cardiovascular, respiratory, gastrointestinal and renal systems are all affected **Cakir et al., 2004**. Importantly, immediately after a burn the natural microbial flora of the skin surface is removed. This makes the wound prone to infections. It has been found that as the burn wound is bigger and deeper, with the dermis being partially destroyed, the risk of subsequent burn wound colonization and infection is increased **Kooistra et al., 2009**.

When treating burn wounds topically, silver sulfadiazine (SSD) is frequently utilized as an antibacterial agent. The SSD products that are now on the market are often offered as 1% w/w creams. According to various researcher the disadvantages of the current commercial SSD products include immediate burst release of the drug into the exposed targeted areas, increased frequency of application (usually two to four times daily), increased inflammation caused by the product's vehicles, cytotoxicity towards keratinocytes and fibroblasts, pseudo eschar formation, and heavy metal poisoning in the event of long-term usage. The sensitivity has increased due to the negative impacts of SSD's sudden burst release.

Exposing the skin to sunlight, skin lesions, severe burn wound itching, skin rashes, blistering, peeling, or loosening of the skin, allergic responses, and cytotoxicity. Each of these helps to slow down the healing process. As a result, a different approach is needed to manage SSD release rates and increase medication efficacy.

Medical researchers' main challenge with targeted drug delivery systems is "how to target them to the right place in the body." and "How to manage the drug's release?" in order to avoid overdosing. These issues might be resolved by the creation of novel molecules like

nanosponges. Nanosponges are tiny, porous structures that resemble sponges and can be used to encapsulate or suspend a wide range of chemicals before adding them to a dosage form. Due to their inclusion and non-inclusion behaviour, they offer a very high solubilization potential for medicines that are weakly soluble and have a spherical colloidal character. Recently, nanosponges have been created, and they are helpful in the transport of drugs. It is possible for nanosponges to solubilize weakly water-soluble drugs, resulting in enhanced drug bioavailability and extended release. Because of their exterior hydrophilic branching and internal hydrophobic chambers, nanosponges offer remarkable versatility in loading both hydrophilic and hydrophobic medicinal molecules.

2. Materials and Methods

2.1. Materials

The sample of Silver sulfadiazine (SSD) was procured from SPA Corporation, Udaipur, Rajasthan, India. The Ethyl cellulose (EC) with a viscosity grade of 18-22 cps was procured from Hi-Media Laboratories Pvt. Ltd. in Mumbai, India. Loba Chemie Pvt. Ltd. provided the remaining reagents located in Mumbai, India. The commercially purchased substances were of analytical quality and utilised without any modifications.

2.2. Pre-formulation studies

The API will go through a comprehensive investigation of its physical features, melting point, solubility studies, partition coefficient, maximal absorption characteristics, and drug-excipient interactions in accordance with the methods outlined by **Anurup et al., 2019**.

2.2.1. Physical properties

The organoleptic (pharmaceutical) characteristics of API such as taste, odour, and colour will be determined through physical (human) mode.

2.2.2. Melting point

Into a capillary tube, closing one end, and monitoring the temperature at which the drug melts while using Thiele's melting point equipment. Three readings' averages will be kept track of. **Emmanuel et al., 2013**.

2.2.3. Solubility studies

The solubility of the API will be tested in distilled water, a number of buffer solutions (pH 4.0, pH 7.4, and pH 8.0), ammonia and methanol. Three identical readings will be used to calculate the average. **Fuller et al., 2013**

2.2.4 Determination of λ max

After accurately weighing 10 mg of silver sulfadiazine, it was transferred to a 100 ml volumetric flask. To dissolve the drug and adjust for volume, 0.5M sodium hydroxide solution was added to this mixture as much as 100 millilitres. The concentration of the resulting solution was 100 μ g/ml. After that, they were further scanned in the 200–400 nm range using a twin beam UV–visible spectrophotometer to determine the absorption maxima. **Razavi et al., 2018**.

2.2.5 Calibration curve of Silver sulfadiazine in 0.5M Sodium Hydroxide Solution

The calibration curve of Silver sulfadiazine was prepared in 0.5M Sodium Hydroxide solution. From the 100 μ g/ml solution 0.1, 0.2, 0.3, 0.4, 0.5, 0.6, 0.7, 0.8 and 0.9 ml were withdrawn separately into pre-calibrated volumetric flask of 10 ml volume and 0.5M sodium hydroxide solution was used to bring the volume up to the required level. The absorbance

7.	Water(ml)	100	100	100	100	100	100	100	100	100	100
8.	Drug: Polymer (w/w)	1:1	1:2	1:3	1:4	1:5	1:6	1:7	1:8	1:9	1:10

3.2. Characterization of nanosponges

3.2.1 Physical examination

The colour and texture of the prepared nanosponge compositions were visually inspected. All of these qualities were created using nanosponge compositions.

3.2.2. Drug entrapment efficiency

20 mg of drug-loaded ethyl cellulose NSPs were dissolved in two millilitres of dichloromethane and methanol to create a solution. A 0.05% v/v aqueous ammonia solution (48 ml) was then added to the mixture. For 30 minutes, the resultant liquid was heated to between 50 and 55°C. Using the same aqueous ammonia solution, the final volume was adjusted to 50 ml. Following the chilling and filtering operation, a clear phase was generated. Using a UV-1800 spectrophotometer from Shimadzu, Japan, the sample was subjected to spectrophotometry at a wavelength of 241 nm. The material was suitably diluted with an aqueous ammonia solution before analysis. We assessed the drug content and drug entrapment effectiveness of NSPs. Each exam was run three times, and the

$$\% \text{ Drug entrapment efficiency} = \frac{\text{Actual Drug Content in Nanosponges} \times 100}{\text{Theoretical Drug Content}}$$

3.2.3. Particle size determination

The laser diffraction method (Malvern Mastersizer, Mastersizer 2000, Malvern Instruments, UK) was utilized to evaluate the particle size distribution of SSD nanosponges. Water was employed as the dispersion. The particle size distribution was measured and used to calculate the values of d (0.1), d (0.9), and d (0.5).

3.4. Preparation of nanosponges-loaded emulgel

A 1% w/v Carbopol gel base was created by dispersing 1 g of carbopol 934 in a solution consisting of 95 ml of water and 5 ml of glycerin. The mixture was then let to sit overnight. The scattered mixture was balanced to a pH of 7.0 using triethanolamine in order to create a gel basis. A dose of 40 mg of a medication equal to NSPs was ingested and evenly distributed inside a gel basis weighing 4 g, resulting in a gel containing 4 g of Silver sulphadiazine nanosponge.

3.5. Characterization of nanosponge-loaded emulgel

3.5.1. Physical examination

Colour, appearance, and consistency of the created emulgel compositions were visually checked.

3.5.2 Rheological study: Spindle number 64 and 50 rpm were selected on a Brookfield viscometer (LV DVE, Brookfield Engineering Corporation, USA) in order to determine viscosity. Five gm of emulgel were placed in a 50 ml beaker, which was left until the spindle groove was dipped and the dial reading was taken three minutes later. Using the acquired reading, factor was used to compute viscosity. Three times over the process was done, and the results were noted as mean \pm SD. **Mankar *et al.*, 2022.**

3.5.3. Texture analysis profile

The Texture Profile Analysis (TPA) was conducted using a Brookfield CT3 Texture Analyzer in compression mode, with the spreadability accessory (TA-SF). The gel formulation was carefully put into the female probe, ensuring that no air pockets were introduced into the samples. Each sample was subjected to the insertion of a conical analytical male probe with a diameter of 35 mm and an angle of 45°. The probe was inserted at a constant rate of 1 mm/s and to a depth of 10 mm. Two duplicate analyses of the material were conducted at a temperature of 35°C. The hardness, cohesiveness, and adhesiveness of the emulgel were determined based on the force-time plots. Hardness refers to the force needed to achieve a specific deformation, cohesiveness measures the work required to deform the emulgel during downward movement of the probe, and adhesiveness quantifies the work needed to overcome attractive forces between the sample surface and the probe surface. Spreadability was calculated from the energy required to deform the sample or from the hardness of the sample.

3.5.4. Determination of pH

A solution of 1gm of gel was prepared by dissolving in 30ml distilled water. The pH of the nanosponge based emulgel was determined by the use of a digital pH meter.

3.5.5. Homogeneity and grittiness

A tiny amount of gel was squeezed between the thumb and index finger to observe its consistency, whether it was uniform or not. In addition, the uniformity may be identified by applying a little amount of the gel over the skin of the dorsal side of the hand. The coarseness of the produced gel is also examined in a similar manner.

3.5.6. Drug content

Emulgel formulations of 1.0 g was taken in 100 ml volumetric flask containing 20 ml of ammonia and stirred for 30 minutes allowed to stand for 24 hours in case of nanosponge loaded emulgel formulations. The resulting solution was passed through a membrane filter. The solution's absorbance was measured spectrophotometrically at 262 nm.

3.5.7 Zeta potential analysis

Zeta potential analysis was done for determining the colloidal properties of the prepared formulations. The suitably diluted nanoemulgel dispersion was determined using zeta potential analyzer based on Electrophoretic light scattering and laser Doppler Velocimetry method. The temperature was set at 25 °C. Charge on vesicles and their mean zeta potential values were measured

3.5.8. Surface morphology by scanning electron microscopy (SEM)

Using a scanning electron microscope, the surface morphology of the nanoemulgel was ascertained. Nanosponges was coated with Gold-palladium alloy of 120°A Knees on the sample sputter coating unit (Model E5 100 Polaron UK) and their surface morphology were photographed with Jeol JSM-T330A, Japan Scanning electron microscope.

3.5.9. Differential scanning calorimetry (DSC)

The DSC profile of pure sulfadiazine was recorded on DSC Q20 (TA Instruments, U.S.A). Thermal behaviour was studied under normal conditions with perforated and sealed quartz pans and with a nitrogen gas flow of 200 ml/min. The sample was heated at 5° C/min over a temperature range of 35-300 ° C. The reference sample used for all the analysis was alumina bearing a height of 5 mg. Thermograms containing peak temperatures and enthalpies were calculated with reference to reported data.

3.6. Transmission Electron Microscopy (TEM) Study

TEM analysis of Silver sulphadiazine nanoparticles was done by using FEI Tecnai G2 F20 model (The Netherlands) operating at 200kV. Sample was prepared by loading one drop of sample on carbon coated Copper grid and was allowed to air dry for 30 min and analyzed at various angles (Uma devi et al., 2013).

3.7. X-ray diffraction

The crystallinity of carbamazepine was monitored before and after encapsulation into the nanosponges. This was achieved using an X-ray powder diffractometer (Bruker MeasSrv-D2-208219/D2-208219) which employed secondary graphite monochromated at 30 kV/10 mA. The data were collected at a scanning steps of 0.03° to cover the two-theta range of $3-60^\circ$ at a temperature (Abdalla et al., 2021)

3.8. In-vitro diffusion study

A research on the release of substances outside of a living organism was conducted using a Franz diffusion cell. The cell consisted of a compartment that received the released substances, which had a volume of 25 ml. The area across which the substances diffused was 3.14 cm^2 . The cellulose dialysis membrane 150 LA401-1MT (Himedia, Mumbai, India) was immersed in receptor media (phosphate buffer, pH 7.4) for duration of 24 hours before to the experiment. A pre-established quantity of gel containing nanosponges was applied to the donor side. The receptor media was agitated constantly at a speed of 50 revolutions per minute and maintained at a temperature of $32 \pm 0.5^\circ\text{C}$ using a water jacket. At specified time intervals, 1 ml samples were extracted from the receiver compartment and substituted with an equivalent amount of new buffer. The gathered samples were examined using a UV spectrophotometer at 262 nm.

3.8.1 Release kinetics

Various equations, such as the zero-order rate equation, which describes the system where release rate is independent of the concentration of the dissolved species, were employed to characterize the kinetics of the drug release process in all formulations. The release from systems where the concentration of the dissolving species determines the dissolution rate is described by the first order equation. The release from a system in which a solid drug is distributed throughout an insoluble matrix is described by the Higuchi equation, and the rate of drug release is correlated with the rate of diffusion.

In Korsmeyer-Peppas model, the diffusional exponent, is n , indicates the drug release mechanism. A value of $n = 0.45$ indicates Fickian or case I release; $0.45 < n < 0.89$ indicates non-Fickian or anomalous release; $n = 0.89$ indicates. The Korsmeyer-Peppas equation is used to analyze whether the release of mechanism is Fickian diffusion, non-Fickian diffusion. 'n' value could be used to characterize different release mechanisms. Korsmeyer-Peppas equation is as follows

$$\% R = K t^n \text{ Or } \log \% R = \log K + n \log t$$

Where, R=drug release,

n =slope,

K=constant,

t =time

a) Zero order kinetics

Drug dissolution from pharmaceutical dosage forms that do not disaggregate and release the drug slowly, assuming that the area does not change and no equilibrium conditions are obtained can be represented by the following equation.

$$Q_t = Q_0 + K_0 t$$

Where, Q_t = Amount of drug dissolved in time 't',

Q_0 = Initial amount of drug in the solution and

K_0 = Zero order release constant

b) First order kinetics

The release rate data were fitted to the following equation in order to investigate the first order release rate kinetics.

$$\log Q_t = K_1 t / 2.303 + \log Q_0$$

Where, Q_t = Amount of drug released in time t,

Q_0 = Initial amount of drug in the solution and

K_1 = First order release constant

c) Higuchi model

Higuchi created a number of theoretical models to investigate the release of medications that are low- and water-soluble when mixed with semisolids or solid matrices. It was possible to derive mathematical formulas for drug particles distributed in a homogeneous matrix acting as the diffusion media. The equation of Higuchi

d) Korsmeyer-Peppas release model

To study this model the release rate data is fitted to the following equation

$$M_t/M_\infty = K \cdot t^n$$

Where, M_t / M_∞ = Fraction of drug release,

K = Release constant & t = Drug release time

In order to study the release of drugs that are water- and low-soluble when combined with semisolids or solid matrices, Higuchi developed a number of theoretical models. For the drug particles arranged in a homogeneous matrix serving as the diffusion media, mathematical formulas might be derived. The Higuchi equation

% Cumulative Drug Release v/s Time (Zero order rate kinetics).

Log % Cumulative Drug Retained v/s Time (First order rate kinetics).

% Cumulative Drug release was plotted against T (root time).

(Higuchi model) Log % Cumulative Drug Release v/s Log Time (Peppas exponential equation)

3.9. In-vivo studies

Male Wistar albino rat in good health weighing between 250-275 gm were chosen. The Institutional Animal Ethics Committee examined and approved all experimental techniques and protocols used in this investigation. The animals were categorized into six groups, each consisting of six rats, as follows:

- I) Group I represent the normal control group with no burn.
- II) Group II consists of negative control group wound created but not treated.
- III) Group III includes positive control group in that wound treated with 1% standard silver sulphadiazine cream.
- IV) Group IV comprises wound treated with optimised nanosponges loaded emulgel 1.

V) Group V include wound treated with optimised nanosponges loaded emulgel 2.

VI) Group VI wound treated with nanosponges loaded emulgel without drug.

In order to induce a wound, the rats were sedated and their back hairs were shaved. The area where the wound was to be created was then marked with a pen before removing the skin. Each rat was wounded with a 300 mm² of area. The wounds were cleansed daily using sterile

normal saline. Following the cleansing process, an adequate quantity of gel was uniformly administered once daily to completely cover the whole wound. The wound area was measured on days 0, 5, 10, 15 and 21. The area of each wound was properly estimated.

3.9.1. Acute skin irritation study

Acute skin irritation and toxicity investigations of the optimized formulation were performed on Newzeland white rabbit following the OECD standards 402 (OECD, 1987). The shaved backs of rabbits were treated with optimised formulation and observed for aberrant skin reactions such as irritation, erythema, and edema for 24, 48, and 72 hrs. The skin that was exposed to a solution containing 0.2% formaldehyde was utilized as the positive control. The scores were documented in accordance with the Draize patch test.

3.9.2. Burn Wound Model

The male wistar albino rat from the Wister strain, weighing between 250-275 gm, will be separated into six groups, including a control group. i) Normal Control group with no expected response ii) Negative control group wounds created but not treated (iii) Positive control (iv) Test-1 (optimised) (v) Test-2 (optimised) and vi) Only polymer containing emulgel. Partial thickness burn wounds will be created on animals that have been fasting overnight. The animals will be under anaesthesia using pentobarbitone at a dosage of 30 mg/Kg administered intraperitoneally. The burns will be inflicted by pouring hot molten wax at a temperature of 80°C into a cylinder with circular perforations of 300 mm². The cylinder will be put on the shaved back of the animal until the wax solidifies. After about 10-12 minutes, the cylinder containing wax will be taken off, revealing a distinct circular burn wound of partial thickness of 300 mm². Following the damage and in the days that follow, the medications or vehicle will be administered topically without delay. With the exception of the medicine being studied, no local or systemic chemotherapeutic treatment will be given to the animals. (Cai et al, 2014; Lambebo et al, 2021).

3.9.3. Assessment of wound healing area

The evaluation of wound healing will be conducted based on the percentage of wound contraction and the duration of epithelization. **Pattnaik et al.,2023**. The percentage of wound contraction will be determined by using the following formula, where the starting size of the wound is taken as 100%.

$$\% \text{ wound contraction} = \frac{\text{Initial wound area} - \text{Specific day wound area}}{\text{Initial wound area}} \times 100$$

Initial day wound area

3.9.4. Determination of Hydroxyproline

Hydroxyproline (HPR) is a compound. 0.3 mL of hydrolysate, 2.5 N NaOH, 0.01 M CuSO₄, and 6% H₂O₂ will be added to each tube. The tubes will be forcefully agitated and promptly immersed in a water bath at a temperature of 80 degrees Celsius. After duration of 15 minutes, the tubes will be extracted and allowed to cool for a period of 5 minutes in cold water. A total of 0.6 mL of a recently made 5% solution of Para dimethyl amino-

benzaldehyde in *n*-Propanol, along with 1.2 ml of 3 N H₂SO₄, will be included. The test tubes will be repositioned in a hot water bath at a temperature of 75°C for duration of 15 mins, followed by a cooling period of 5 mins under a flowing stream of water. The intensity of colour will be quantified at a wavelength of 540 nm relative to a blank sample. The hydroxyproline content in the tissue will be determined using a standard curve established with a standard 4-Hydroxy-*L*-proline ranging from 75 to 900 µg/0.3 ml. This will be done using a working solution with a concentration of 3 mg/ml. (Murthy et al, 2013, Newman and Logan, 1950).

3.9.5. Histopathological study

Tissue samples will be collected on Days 0, 5, 10, 15, and 21 from all five animal groups for histopathological analysis. The specimens will be preserved in formalin and mounted on slides, then stained with haematoxylin and eosin, and finally examined using a light microscope. The measured variables included scar formation, presence of inflammatory cells, development of new blood vessels, congestion, density of collagen produced by fibroblasts, presence of fibrin, and aggregation of fibroblasts. Fatima et al.,2021.

3.9.6 Statistical analysis

Results were subjected to two-way ANOVA followed by Bonferroni post-tests (***p<0.001 Vs control group; **p<0.01 Vs control group; *p<0.05 Vs control group) was considered significant.

3.9.7. Accelerated stability study

Accelerated stability testing studies was performed for 6 months. The optimized formulations were kept at 40 ± 2 °C and 75 ± 5% RH. Physical appearance, drug content and % drug release were fixed as evaluation parameter for stability study.

4. RESULTS & DISCUSSIONS

4.1. Pre-formulation studies

4.1.1 Physical properties

Result of physical characterization of Silver sulphadiazine is listed in Table. Variations were found in its specification in Certificate of Analysis (COA) and observations recorded at the time of experimentation.

TABLE: 2. Physical properties of Silver sulphadiazine

Odour	Odorless
Colour	White
Appearance	Powder

4.1.2 Melting point

Experimentally observed melting point complies with reported melting point in COA, Sigma-Aldrich, India.

Table:3. Melting point report of Silver sulphadiazine

Sl. No.	Reported	Observed		
1	253°C-255°C	Trail-I	Trail-II	Trail-III
		253.5 °C	253.6 °C	254 °C

4.1.3 Solubility analysis

Silver sulphadiazine was soluble in ammonia and dimethyl sulphoxide. Slightly soluble acetone and ether. Practically insoluble in water and ethanol.

4.1.4 Determination of λ max

Calibration curve of Silver sulfadiazine was developed in 0.5M NaOH solution. Reason behind selecting above mentioned solution is its solubility criteria and its wide acceptance in USP monographs.

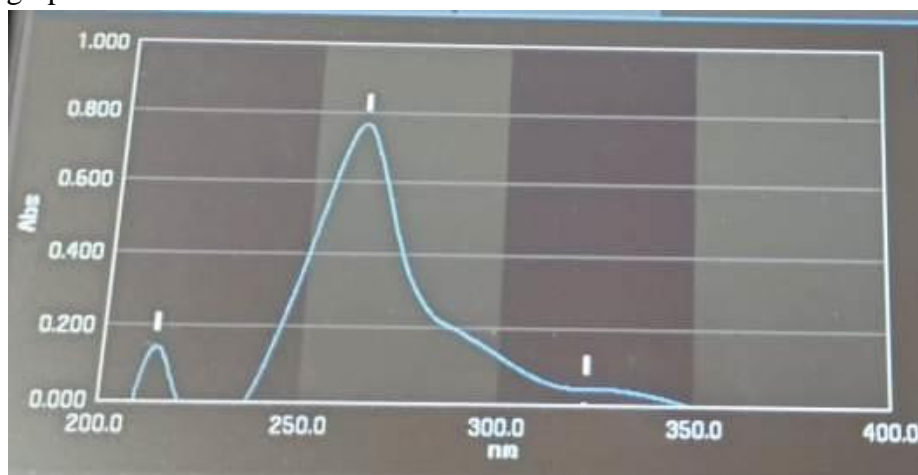


Figure:1. Absorption maxima peak

4.1.5 Standard calibration curve of Glipizide

Silver sulphadiazine obeys the Beer's law in concentration range of 1-9 $\mu\text{g/ml}$ in 0.05 M NaOH solution with regression of coefficient (r^2) 0.9992. The calibration data is given in Table 4 and calibration curve was constructed in Fig.1.

Table:4. Silver sulphadiazine calibration curve data

Sl. No.	Concentration($\mu\text{g/ml}$)	Absorbance at 262 nm
1	1	0.0210
2	2	0.149
3	3	0.259
4	4	0.402
5	5	0.528
6	6	0.670
7	7	0.814
8	8	0.946
9	9	1.058

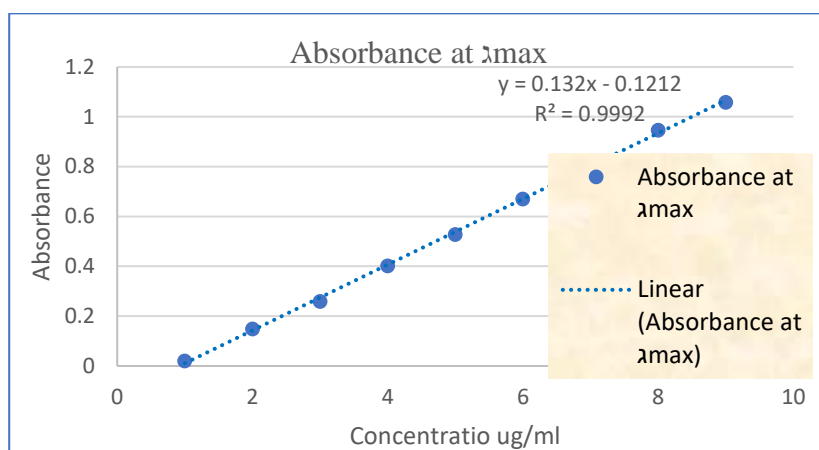


Figure: 2. Calibration curve of Silver sulfadiazine in 0.5M NaOH solution

4.1.6 FTIR interpretation

The FTIR spectra of the drug and its excipients were obtained using the potassium bromide disc technique using an FTIR spectrophotometer. The drug was identified by infrared spectroscopy and characteristics peak obtained compared with spectra of Silver sulfadiazine, ethyl cellulose, Xanthan gum, polyvinyl alcohol, nanosponge gel, physical Mixture etc.

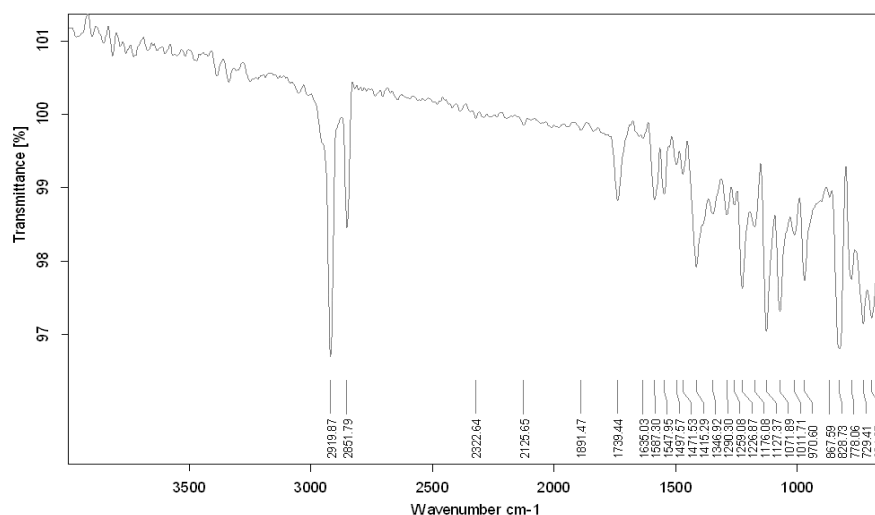


Figure: 3. FTIR spectra of Silver Sulphadiazine

Table:5. FTIR interpretation of pure drug

Functional group	Frequency cm-1
Hydroxyl group	2919.87
C=O	1739.44
Carbonyl groups of acids	1415.29
C-O-C group	1127.37
C-C1	729.41

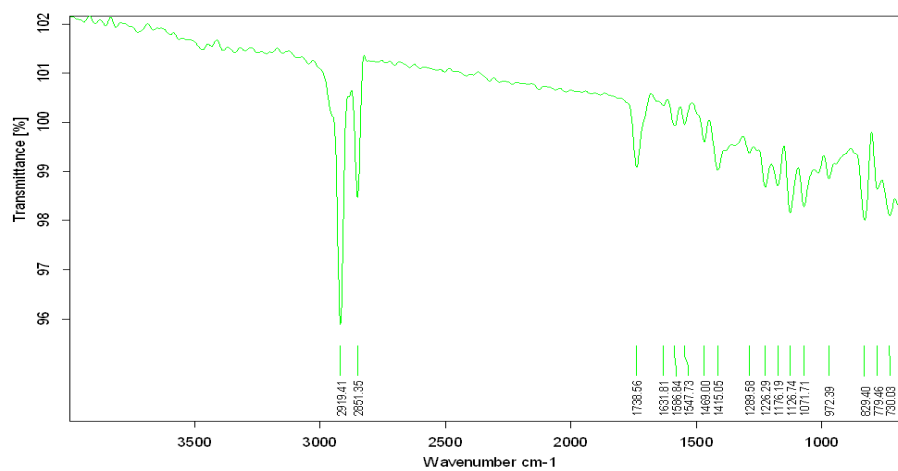


Figure: 4. FTIR spectra of Ethyl cellulose

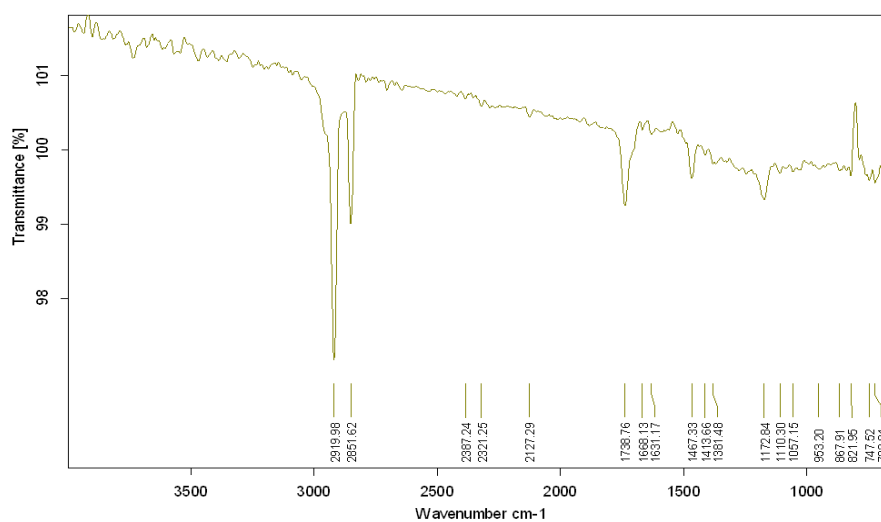


Figure: 5. FTIR spectra of polyvinyl alcohol

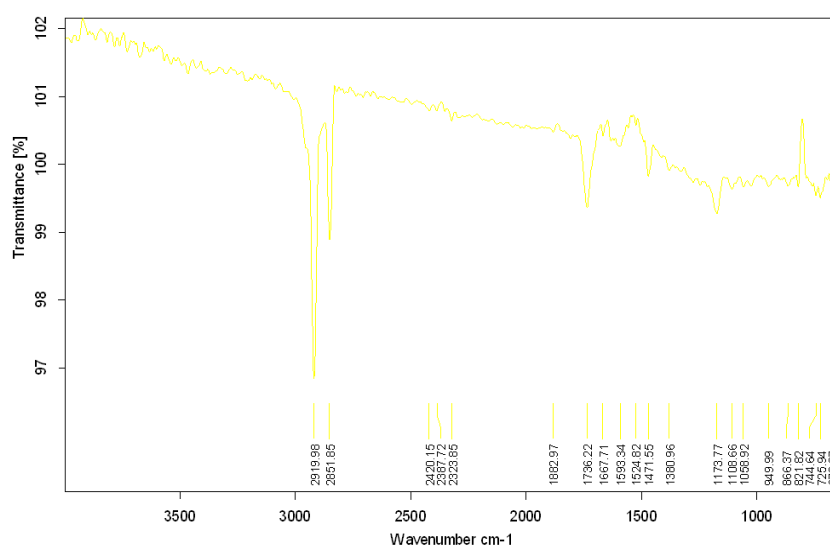


Figure:6. FTIR spectra of Physical Mixture

Table:6. FTIR Data interpretation of silver sulphadiazine, ethyl cellulose xanthan gum and polyvinyl alcohol

Functional group	Frequency cm ⁻¹		
	Range	Pure drug	Physical Mixture
Hydroxyl group	3000-2900	2919.87	2919.98
C=O	1750-1650	1739.44	1736.22
Carbonyl groups of acids	1450-1400	1415.29	1471.55
C-O-C group	1160-1180	1127.37	1106.66
C-C1	800-600	729.41	725.94

4.1.7 Differential scanning calorimetry

With DSC, it is possible to measure the small energy changes that occurs as matter undergo thermotropic transitions with heating from initially in solid to liquid phase. In this study, DSC thermogram for Silver sulphadiazine was determined with DSC Q20 (TA Instruments, U.S.A) and sample size was 1.00 mg. DSC curve of sulfadiazine provides a sharp exothermic peak at 261.34°C indicating its microcrystalline nature. Silver sulfadiazine DSC thermogram the absence of peaks indicates that silver nanoparticles and sulfadiazine have conjugated, as both powders' crystallinity has diminished and may have transformed into an amorphous state. (Fig.7)

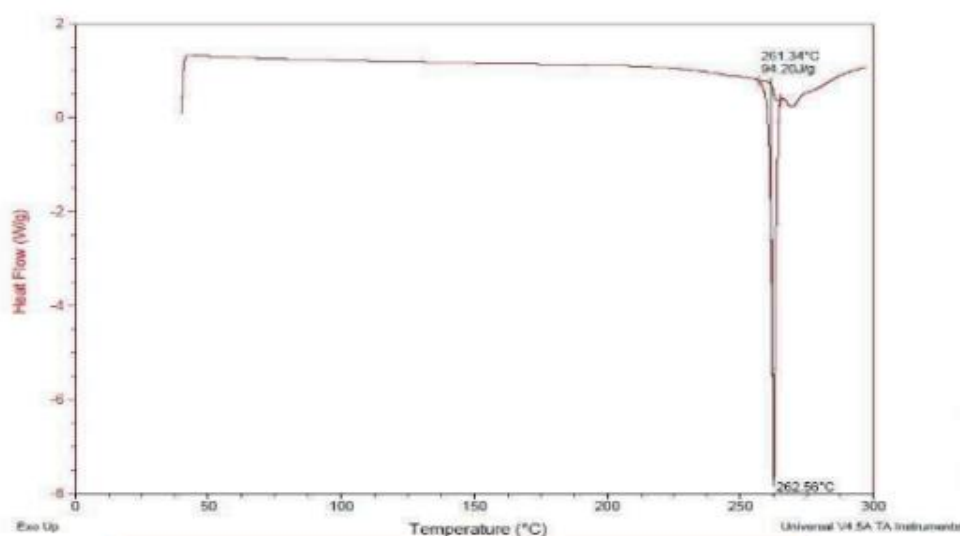
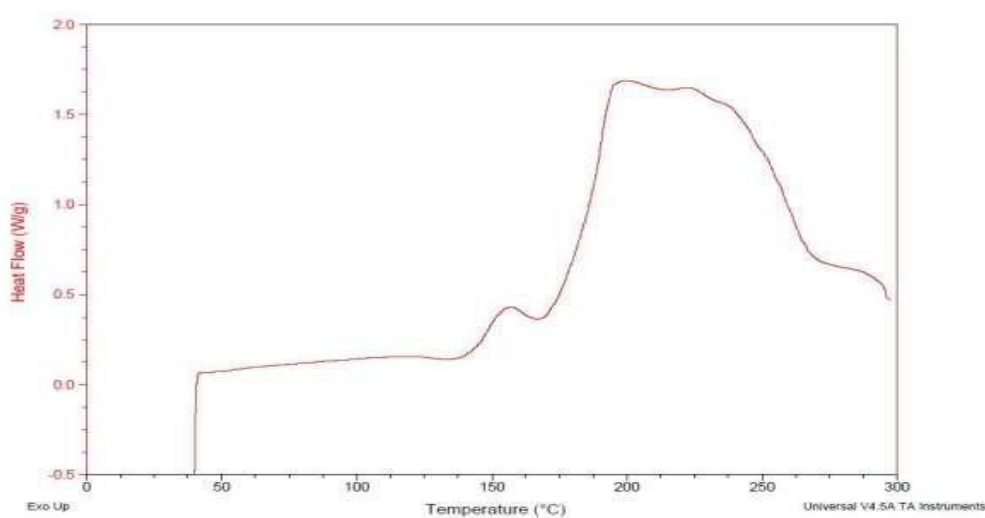
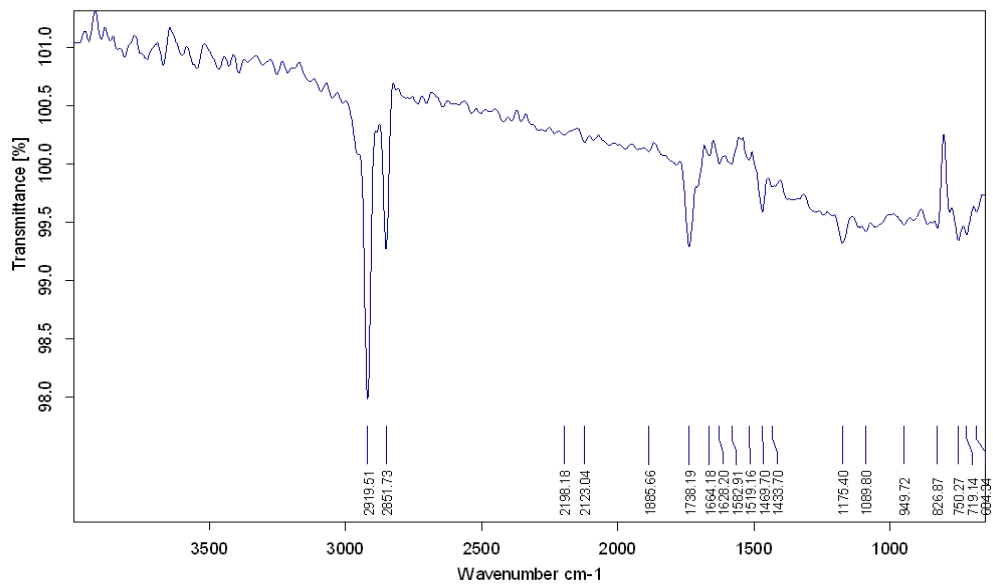
**Figure:7.** DSC thermogram of pure drug

Figure:8. DSC thermogram of physical mixture**Figure:9.** FTIR spectra of Silver sulphadiazine nanosponge 1**Table:7.** FTIR interpretation Silver sulphadiazine nanosponge 1

Functional group	Frequency cm-1
Hydroxyl Group	2919.51
C=O	1738.19
Carbonyl groups of acids	1433.70
c-o-c group	1175.40
Aromatic and Amines	826.87
C-Cl	604.94

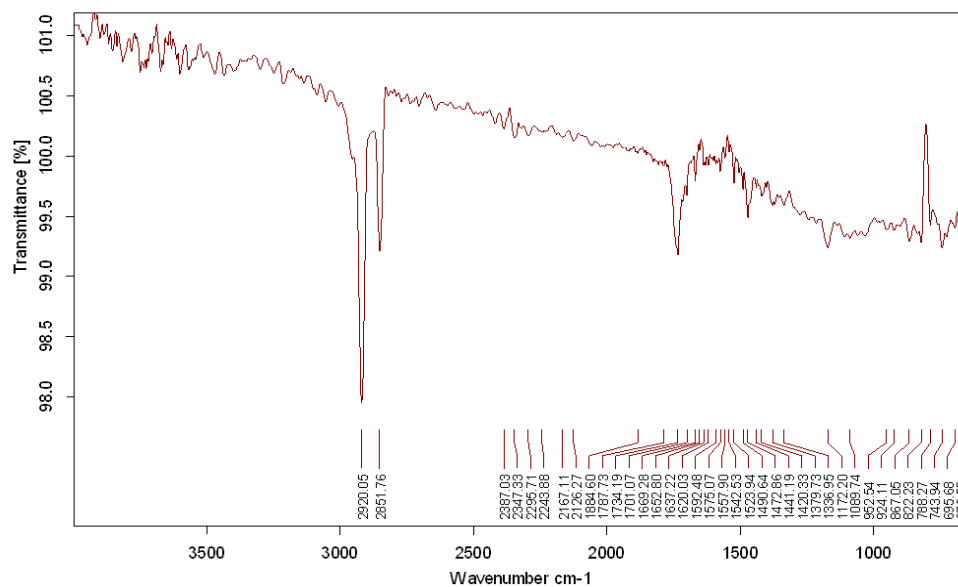


Figure: 10. FTIR spectra of Silver sulphadiazine nanosponge 2

Table:8. FTIR interpretation Silver sulphadiazine nanosponge 2

Functional group	Frequency cm^{-1}
Hydroxyl Group	2920.05
C=O	1734.19
Carbonyl groups of acids	1441.19
c-o-c group	1172.20
Aromatic and Amines	822.23
C-C1	695.68

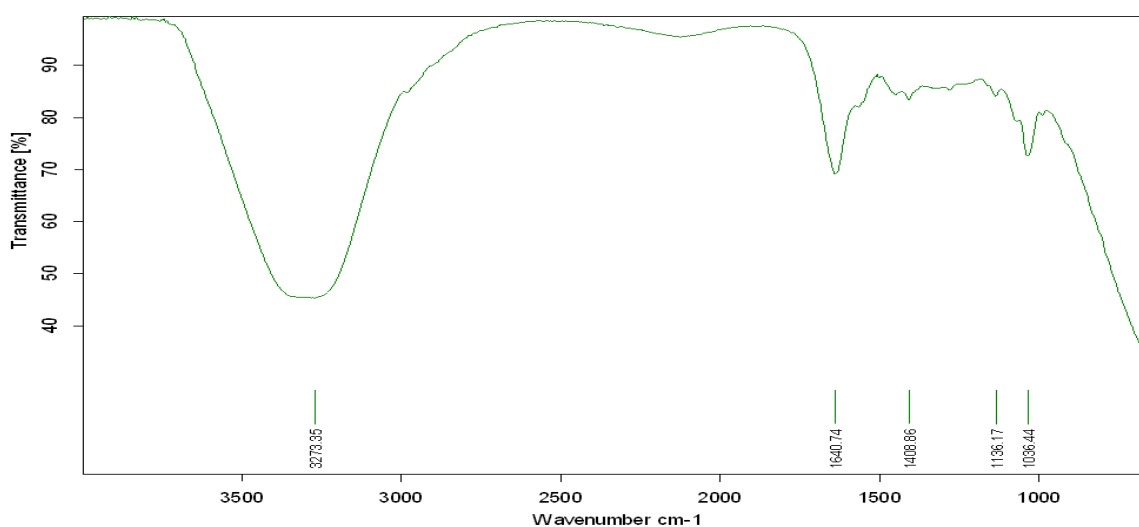


Figure: 11. FTIR spectra of Silver sulphadiazine nanosponge gel 1

Table:9. FTIR interpretation Silver sulphadiazine nanosponge gel 1

Functional group	Frequency cm^{-1}

Hydroxyl Group	3273.35
C=O	1640.74
Carbonyl groups of acids	1408.86
c-o-c group	1136.17
Aromatic and Amines	1036.44
C-Cl	-

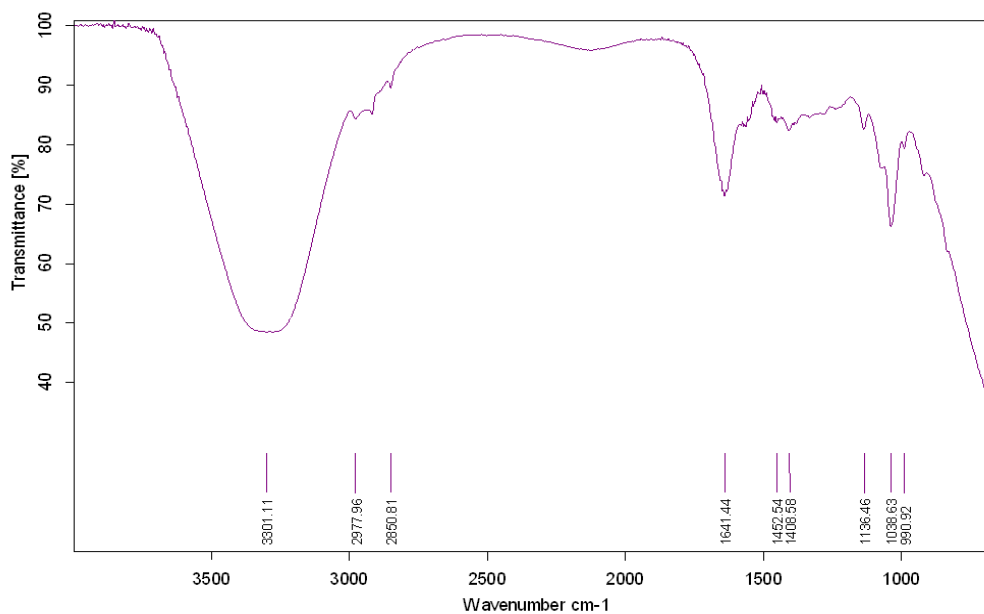


Figure: 12. FTIR spectra of Silver sulphadiazine nanosponge gel 2

Table:10. -FTIR Data interpretation of Silver sulphadiazine nanosponge gel 2

Functional group	Frequency cm-1
Hydroxyl Group	2977.96
C=O	1641.44
Carbonyl groups of acids	1452.54
c-o-c group	1136.46
Aromatic and Amines	990.92
C-Cl	-

Table:11. pH, Viscosity (cps) and drug content of nanoemulgel of optimised formulation

Formulation code	pH	Viscosity in (cps)	%Drug content
F4	5.4	11,357	92.90

F10	5.8	11,435	95.26
------------	-----	--------	-------

4.1.8 Drug loading and entrapment efficiency

The concentration of the drug in the dispersion medium can be used to gauge the entrapment efficiency of the NSGs system. It was therefore necessary to quantify the active agent. Poorer polymer content in the NSG formulations leads to poorer entrapment efficiency, and process diffusion distributes the active ingredient into the shell of the NSG polymer core. The % drug loading of SSD-NSGs varied from 20.66±1.093% to 34.26±1.017%, while the encapsulation efficiency ranged from 73.73±1.89% to 92.49±0.88%. Encapsulation efficiency was shown to decrease in batches with greater XM concentrations. Here, with batch F10, the highest drug encapsulation was discovered.

Table:12. Percent drug encapsulation and drug loading of nanosponges

Run	SSD: XM (% w/w)	% drug Encaencapsulation	Unentrapped drug (%)	Drug loading (%)	Solubility (µg/ml)
F1	1: 10	81.76±2.41	18.24±2.41	26.71±0.627	66.99±1.820
F2	1: 10	87.91±1.42	12.09±1.42	29.83±0.281	55.30±1.235
F3	1: 20	86.97±1.89	13.03±1.89	28.19±0.814	70.12±0.284
F4	1: 20	91.49±0.88	7.02±0.80	30.26±1.019	140.74±4.738
F5	1: 15	83.66±1.42	16.34±1.42	25.99±0.516	94.60±1.002
F6	1: 10	77.51±1.90	22.49±1.90	22.65±2.017	85.45±1.912
F7	1: 15	77.34±0.88	21.60±0.88	21.47±1.235	112.21±4.037
F8	1: 20	80.82±1.42	19.18±1.42	25.01±0.918	89.16±1.240
F9	1: 15	73.73±1.89	26.27±1.89	20.66±1.093	98.98±1.288
F10	1: 20	92.49±0.88	7.51±0.88	34.26±1.017	145.74±4.636

(Observed values: Mean ±S.D., n=3)

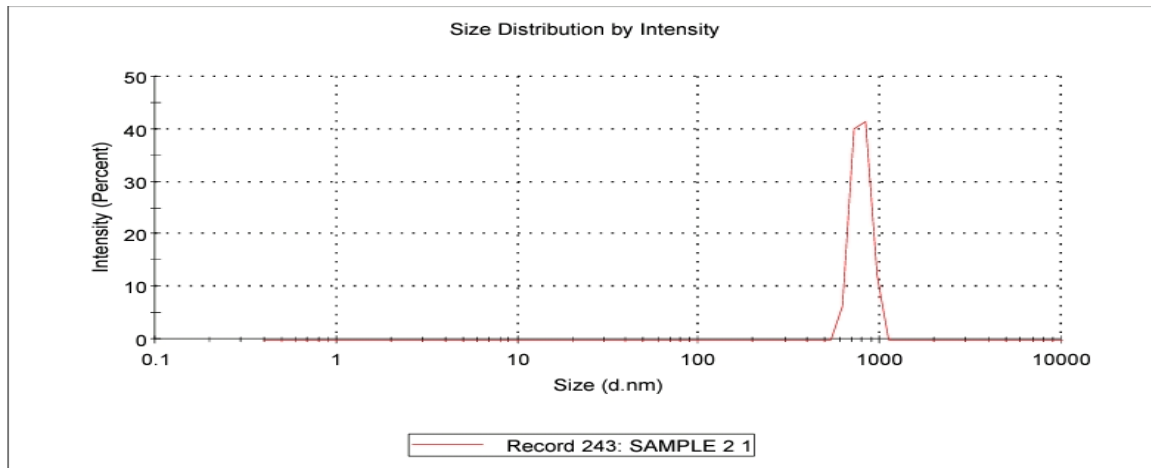


Figure: 13. Particle size distribution of optimized nanosponge formulation 4

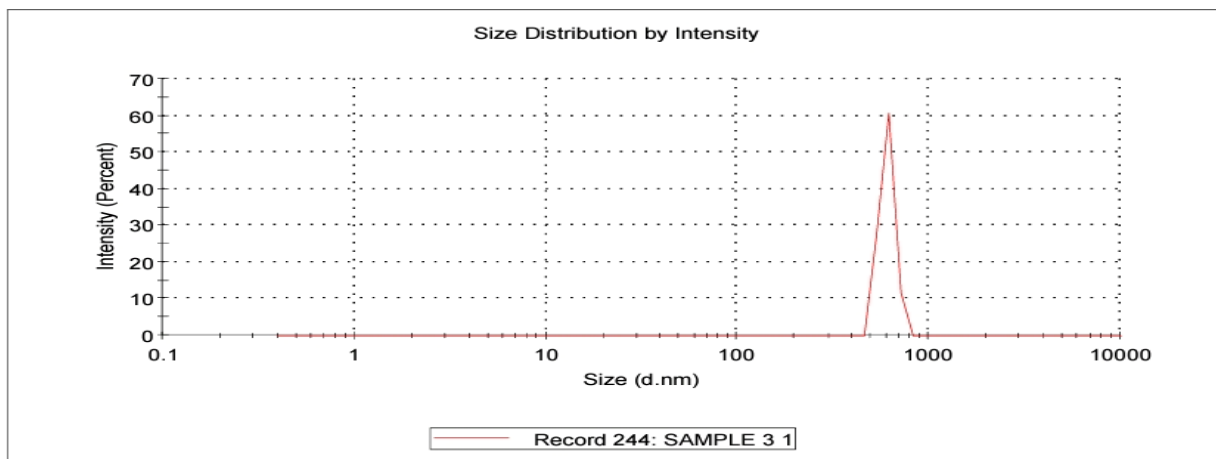


Figure: 14. Particle size distribution of optimized nanosponge formulation 10

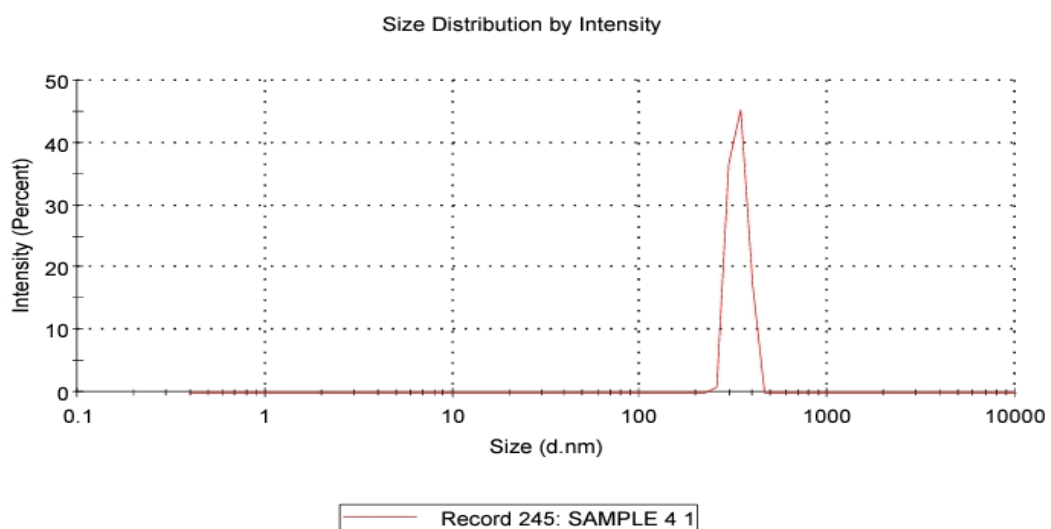


Figure: 15. Particle size distribution of optimized nanoemulgel formulation 4

Z-Average (d.nm): 163.0 **Peak 1:** 191.2 100.0 70.25
Pdl: 0.153 **Peak 2:** 0.000 0.0 0.000
Intercept: 0.887 **Peak 3:** 0.000 0.0 0.000
Result quality: Good

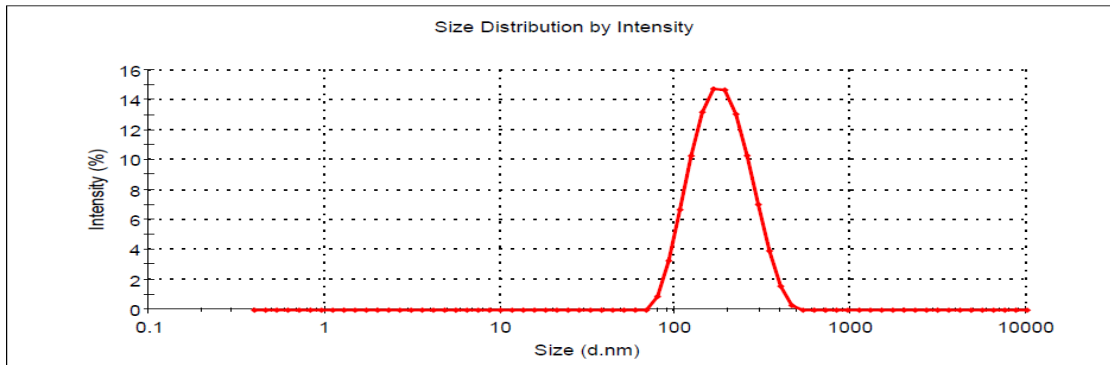


Figure: 16. Particle size distribution of optimized nanoemulgel formulation 10

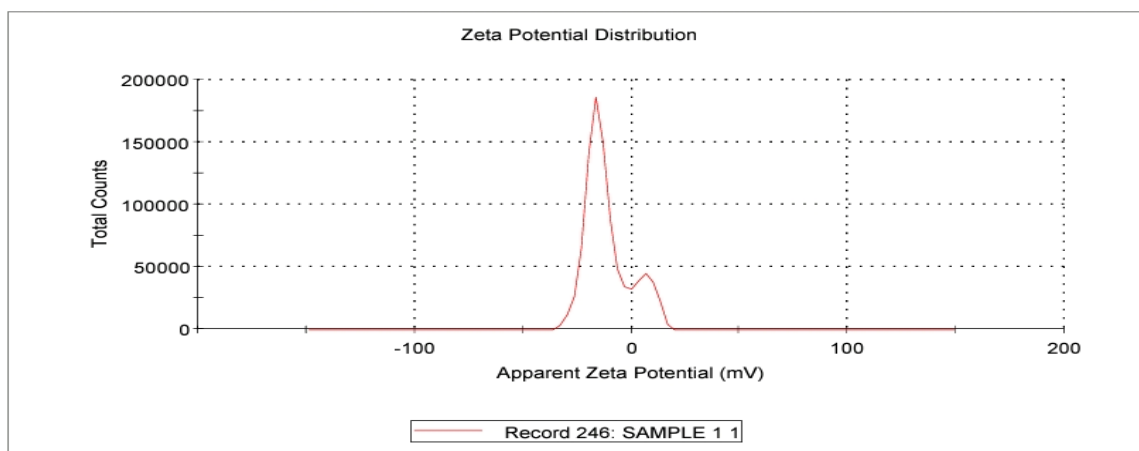


Figure: 17. Zeta potential of nanosponge formulation 4

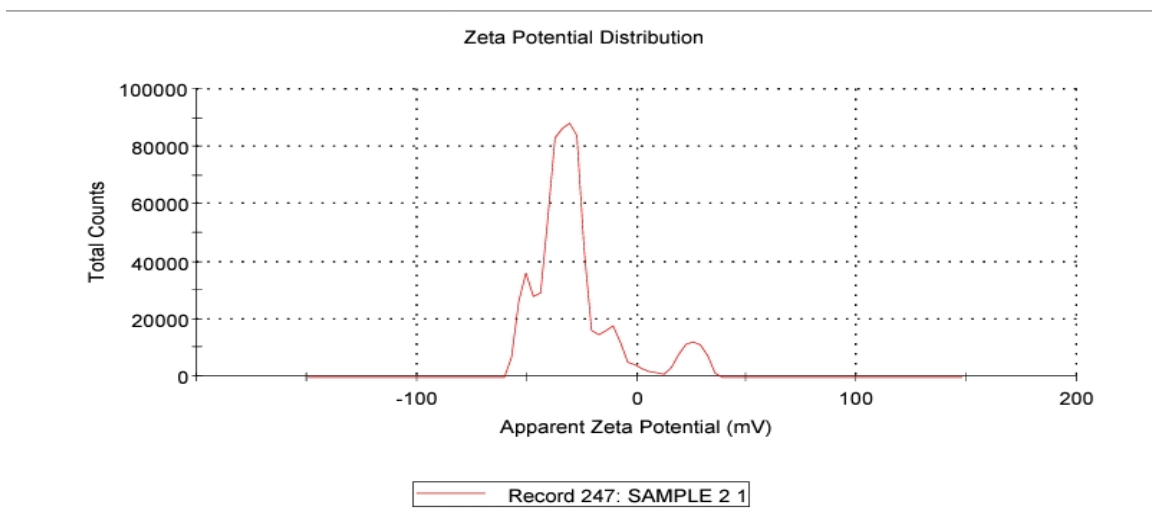


Figure: 18. Zeta potential of nanosponge formulation 10

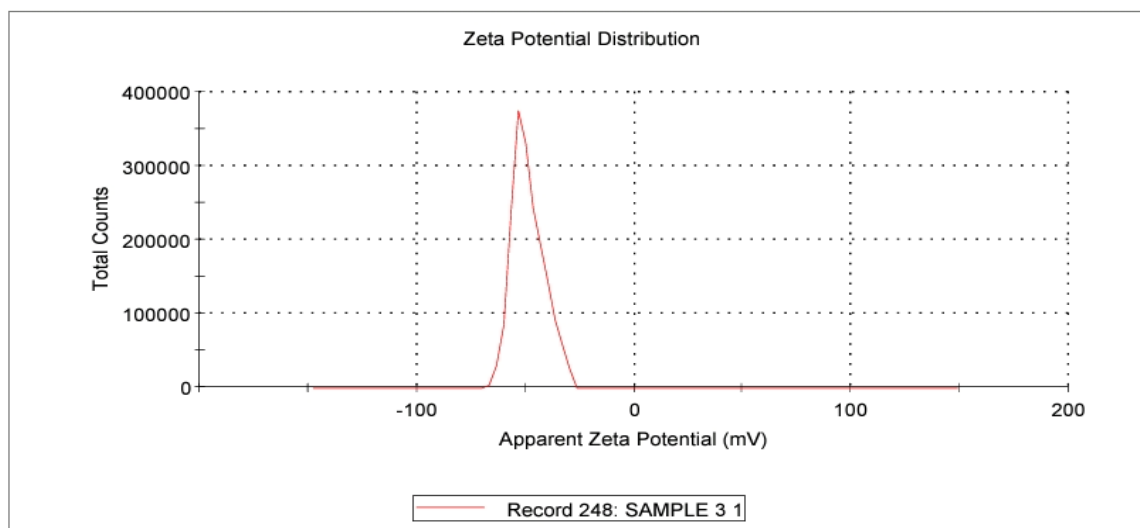


Figure: 19. Zeta potential of optimized nanoemulgel formulation 4

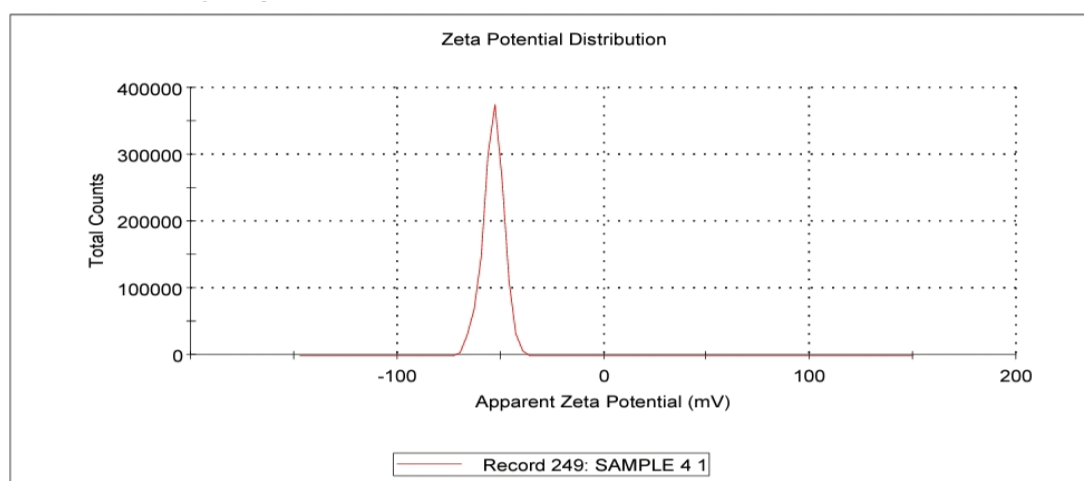


Figure: 20. Zeta potential of optimized nanoemulgel formulation 10

Table:13. The particle size, PDI and zeta potential of Silver sulfadiazine nanospheres prepared with xanthan gum and ethyl cellulose

Formulation Code	Particle size (nm)	PDI	Zeta Potential
F-1	132	0.279	-14.8
F-2	782.4	0.201	-33.0
F-3	603.3	1.000	-48.6
F-4	333.4	1.000	-53.4
F-5	276.5	0.304	-36.5
F-6	164.6	0.173	-27.7
F-7	225.2	0.266	-42.6
F-8	217.8	0.347	-37.8
F-9	384.4	0.243	-43.3
F-10	163	0.153	-36.6

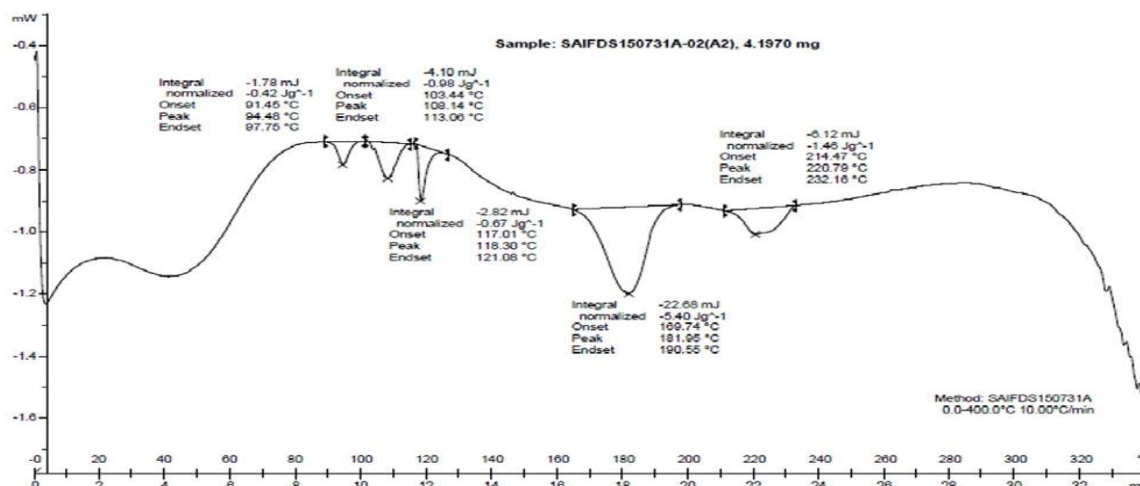
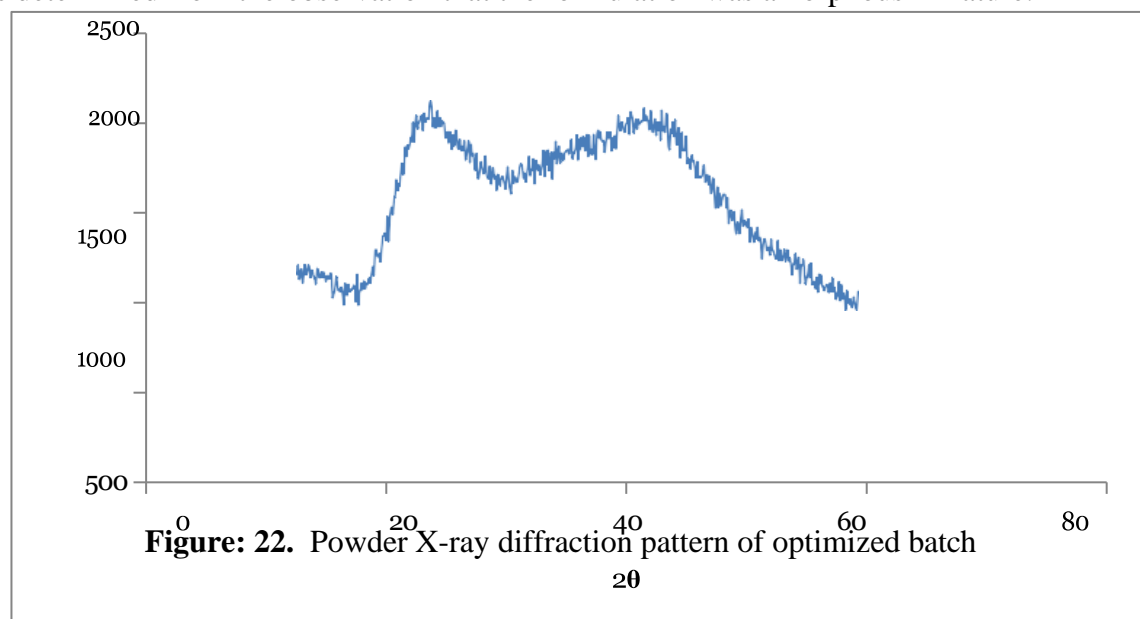


Figure: 21. DSC Thermogram of Silver sulphadiazine Nanosponge

4.1.9 X-ray diffraction

Figure 42. shows the SSDNSGs PXRD diffractogram. A succession of sharp, powerful peaks were visible in the diffractogram linked to the improved formulation. The main characteristic peaks were located at 2θ values of 15.6, 16.8, 17.1, 18.9, 22.6, 41.2, and 43.5°. As a result, it was determined from the observation that the formulation was amorphous in nature.



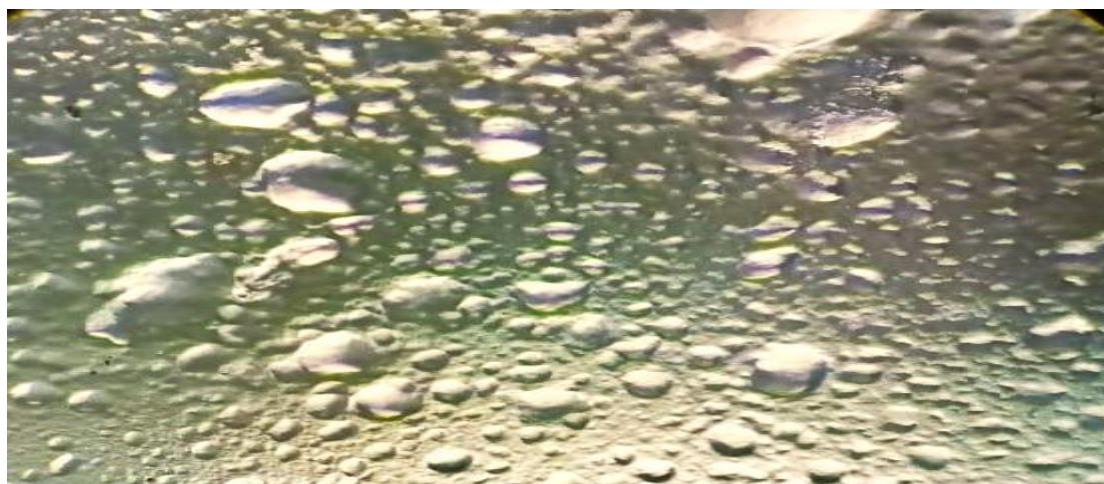


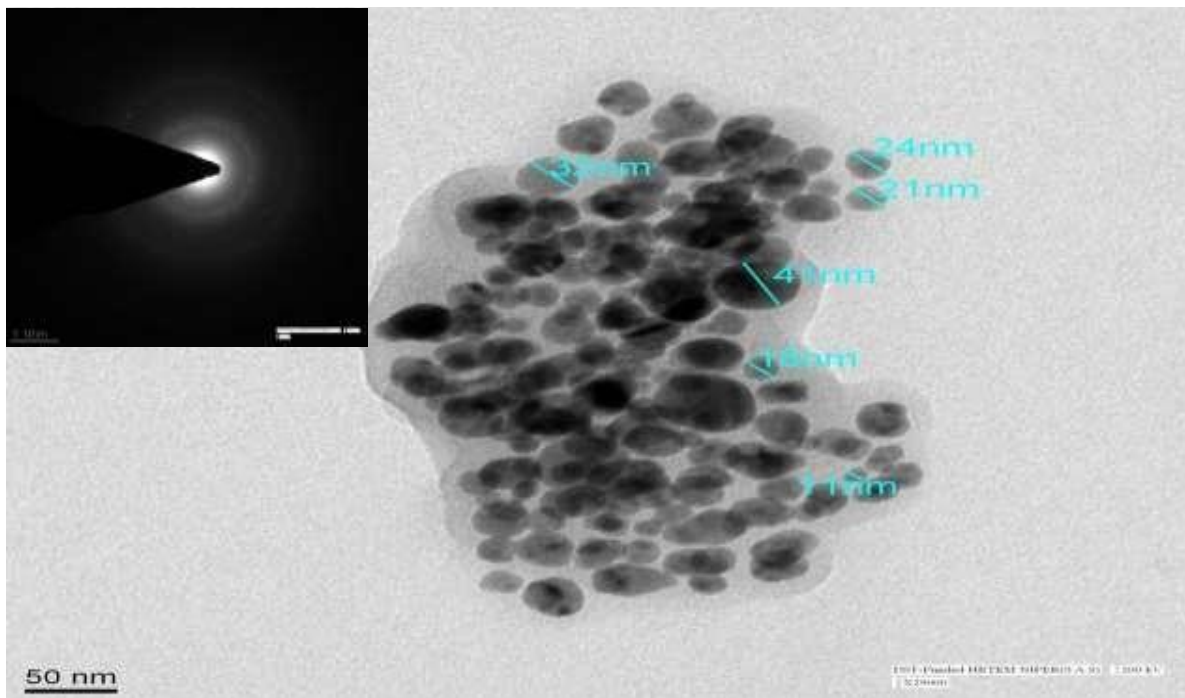
Figure: 23. Microphotographs of optimized nanoemulgel formulation F4



4.2 Transmission Electron Microscopy (TEM)

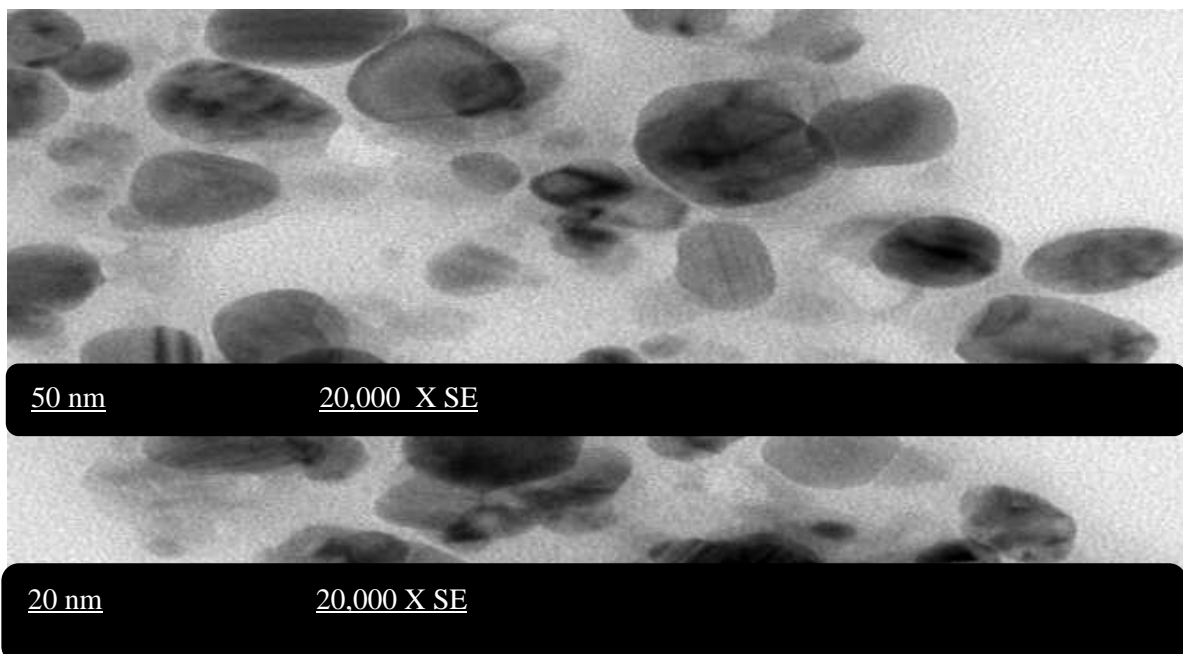
The majority of the particles, according to TEM examination, were between 25 and 100 nm in size. The SAED of one of the aggregated nanoparticles in the silver sulphadiazine nanosponge's selected area electron diffraction pattern (SAED) revealed that the particles were nanocrystalline in nature. In insight of 8.10 (B), SAED dots that matched the various crystallographic planes of the face-centered cubic (fcc) structure of elemental silver are visible. It was discovered that the drug was trapped above the silver sulphadiazine, which was represented as black areas in the structures. The previously mentioned technique was used to conduct a TEM examination of the silver sulfadiazine (SSD) complex.

The SSD particles were discovered to have a spherical-ovoid shape and a particle size in the range of 10–60 nm. It was discovered that the medication was trapped over 60 nm. The

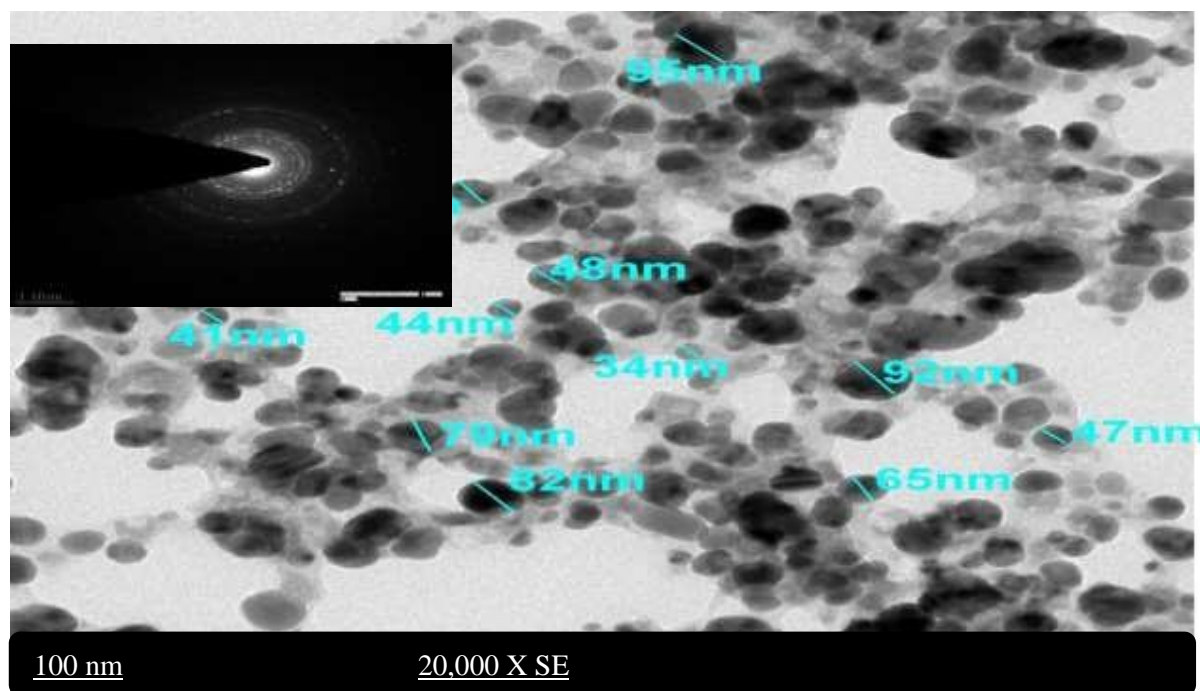


drug was found to be entrapped over the Silver sulphadiazine depicted by black portions in the structures.

Figure: 24. TEM microphotographs of optimized nanoemulgel (Insight SAED image)



(A)



(B)

Figure:25. TEM microphotographs of Silver sulphadiazine (A) 20 nm and (B) 100 nm (Insight SAED image)

4.2.1 Scanning electron microscopy (SEM)

The scanning electron microscope images of nanosponges are shown in figures 1 (a) to 1 (c). The nanosponges that were created had a spherical morphology and possessed a fine mesh-like architecture. The size and form remained unchanged after the encapsulation of the silver sulphadiazine medication inside the nanosponge.

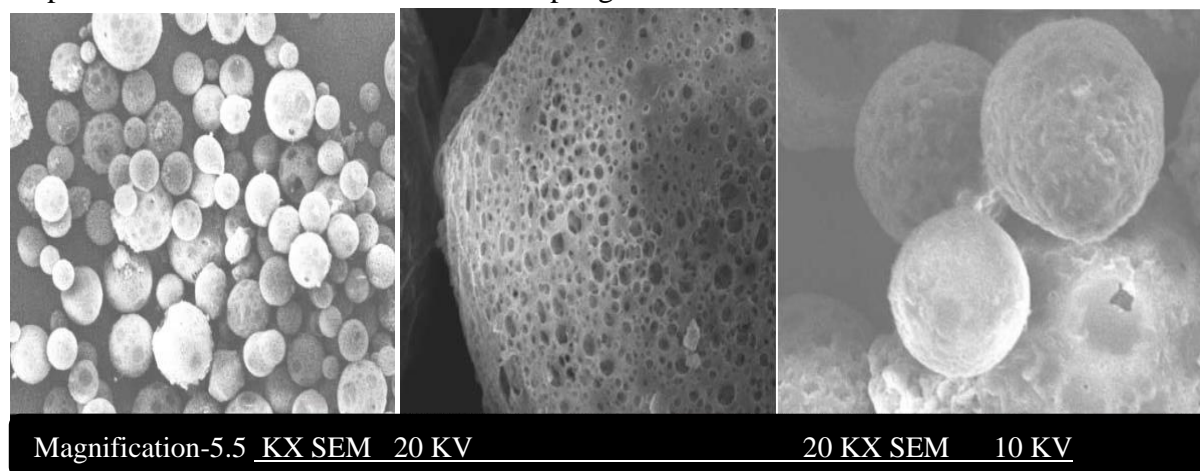


Figure: 26. (1a, 1b, 1c): SEM microphotographs of optimized nanoemulgel formulation

4.2.2 *In-vitro* dissolution study

The release of Silver sulphadiazine from nanosponge based emulgel containing ethyl cellulose and xanthan gum was varied according to their concentration. The progressive decrease in the amount of drug diffused through a dialysis membrane from formulations F1

to F5 and F5 to F10 attributed to gradual increase in ethyl cellulose and xanthan gum content. It has been concluded that, if we increase the concentration of surfactant and polymer the diffusion of drug also decreases. The amount of drug diffused from formulation F4 was showed 47.60% which was lower among the formulations F1 to F5 and F10 was showed 44.64% which was lower among the formulation F5 to F10.

Table:14. Drug dissolution study of nanoemulgel formulation F1 to F5

Time (hrs.)	% Cumulative drug release				
	F1	F2	F3	F4	F5
0	0	0	0	0	0
1	14.3	13.5	12.7	12.3	11.9
2	22.8	19.8	18.1	16.3	15.7
4	29.16	26.0	24.9	22.5	20.62
6	35.23	31.55	27.85	26.7	25.10
8	39.65	36.4	32.25	30.34	28.50
12	44.22	39.22	37.5	34.05	32.10
16	49.16	44.72	42.5	41.5	38.90
20	54.43	51.43	47.4	46.4	44.50
24	58.73	55.65	53.6	49.5	47.60

Table:15. Drug dissolution study of nanoemulgel formulation F5 to F10

Time (hrs.)	% Cumulative drug release				
	F6	F7	F8	F9	F10
0	0	0	0	0	0
1	12.15	10.95	8.12	8.15	7.15
2	18.9	16.8	13.2	12.6	11.60
4	23.2	20.35	18.15	16.55	15.20
6	29.4	27.65	24.65	22.05	20.45
8	34.1	32.65	29.5	26.65	24.36
12	41.23	38.95	34.5	30.05	28.56

16	49.32	47.65	43.23	35.67	34.23
20	54.76	51.54	49.86	42.43	41.10
24	59.35	55.95	53.32	46.55	44.64

Table:16. Release kinetics profile of nanoemulgel formulation F2

Time in (hrs.)	Log T	SQRT	%CDR	Log% Release	%Drug Remaining	Log% Drug Remaining
0	0	0	0	0	100	2
1	0	1	14.3	1.15	85.7	1.93
2	0.30	1.41	22.8	1.35	77.2	1.88
4	0.60	2	29.16	1.46	70.84	1.85
6	0.77	2.44	35.23	1.54	64.77	1.81
8	0.90	2.82	39.65	1.59	60.35	1.78
12	1.07	3.46	44.22	1.64	55.78	1.74
16	1.20	4	49.16	1.69	50.84	1.70
20	1.30	4.47	54.43	1.73	45.57	1.65
24	1.38	4.89	58.73	1.76	41.27	1.61

Table:17. Release kinetics profile of nanoemulgel formulation F3

Time in (hrs.)	Log T	SQRT	%CDR	Log% Release	%Drug Remaining	Log% Drug Remaining
0	0	0	0	0	100	2
1	0	1	13.5	1.13	86.5	1.93
2	0.30	1.41	19.8	1.29	80.2	1.90
4	0.60	2	26.0	1.41	74	1.86
6	0.77	2.44	31.55	1.49	68.45	1.83
8	0.90	2.82	36.4	1.56	63.6	1.80

12	1.07	3.46	39.22	1.59	60.78	1.78
16	1.20	4	44.72	1.65	55.28	1.74
20	1.30	4.47	51.43	1.71	48.57	1.68
24	1.38	4.89	55.65	1.74	44.35	1.64

Table:18. Release kinetics profile of nanoemulgel formulation F4

Time in (hrs.)	Log T	SQRT	%CDR	Log% Release	%Drug Remaining	Log% Drug Remaining
0	0	0	0	0	100	2
1	0	1	12.7	1.10	87.3	1.94
2	0.30	1.41	18.1	1.25	81.9	1.91
4	0.60	2	24.9	1.39	75.1	1.87
6	0.77	2.44	27.85	1.44	72.15	1.85
8	0.90	2.82	32.25	1.51	67.75	1.83
12	1.07	3.46	37.5	1.57	62.5	1.79
16	1.20	4	42.5	1.62	57.7	1.76
20	1.30	4.47	47.4	1.67	52.6	1.72
24	1.38	4.89	53.6	1.72	46.4	1.66

Table:19. Release kinetics profile of nanoemulgel formulation F5

Time in (hrs.)	Log T	SQRT	%CDR	Log% Release	%Drug Remaining	Log% Drug Remaining
0	0	0	0	0	100	2
1	0	1	12.3	1.08	87.7	1.94
2	0.30	1.41	16.3	1.21	83.7	1.92
4	0.60	2	22.5	1.35	77.5	1.88
6	0.77	2.44	26.7	1.42	73.3	1.86
8	0.90	2.82	30.34	1.48	69.66	1.84

12	1.07	3.46	34.05	1.53	65.95	1.84
16	1.20	4	41.5	1.61	58.5	1.76
20	1.30	4.47	46.4	1.66	53.4	1.72
24	1.38	4.89	49.5	1.69	50.5	1.70

Table:20. Release kinetics profile of nanoemulgel formulation F7

Time in (hrs.)	Log T	SQRT	%CDR	Log% Release	%Drug Remaining	Log% Drug Remaining
0	0	0	0	0	100	2
1	0	1	12.15	1.08	87.85	1.94
2	0.30	1.41	18.9	1.27	81.1	1.90
4	0.60	2	23.2	1.36	76.8	1.88
6	0.77	2.44	29.4	1.46	70.6	1.84
8	0.90	2.82	34.1	1.53	65.9	1.81
12	1.07	3.46	41.23	1.61	56.69	1.75
16	1.20	4	49.32	1.69	50.68	1.70
20	1.30	4.47	54.76	1.73	45.24	1.65
24	1.38	4.89	59.35	1.77	40.65	1.60

Table:21. Release kinetics profile of nanoemulgel formulation F8

Time in (hrs.)	Log T	SQRT	%CDR	Log% Release	%Drug Remaining	Log% Drug Remaining
0	0	0	0	0	100	2
1	0	1	10.95	1.03	89.05	1.94
2	0.30	1.41	16.8	1.22	83.2	1.92
4	0.60	2	20.35	1.30	79.65	1.88
6	0.77	2.44	27.65	1.44	72.35	1.85
8	0.90	2.82	32.65	1.51	67.35	1.82
12	1.07	3.46	38.95	1.59	61.05	1.78

16	1.20	4	47.65	1.67	52.35	1.71
20	1.30	4.47	51.54	1.71	48.46	1.68
24	1.38	4.89	55.95	1.74	44.05	1.64

Table:22. Release kinetics profile of nanoemulgel formulation F9

Time in (hrs.)	Log T	SQRT	%CDR	Log% Release	%Drug Remaining	Log% Drug Remaining
0	0	0	0	0	100	2
1	0	1	8.12	0.90	91.88	1.96
2	0.30	1.41	13.2	1.12	86.8	1.93
4	0.60	2	18.15	1.25	81.85	1.91
6	0.77	2.44	24.65	1.39	75.35	1.87
8	0.90	2.82	29.5	1.46	70.5	1.84
12	1.07	3.46	34.5	1.53	65.5	1.81
16	1.20	4	43.23	1.63	56.77	1.75
20	1.30	4.47	49.86	1.69	50.14	1.700
24	1.38	4.89	53.32	1.72	46.68	1.66

Table:23. Release kinetics profile of nanoemulgel formulation F10

Time in (hrs.)	Log T	SQRT	%CDR	Log% Release	%Drug Remaining	Log% Drug Remaining
0	0	0	0	0	100	2
1	0	1.00	8.15	0.911	91.85	1.96
2	0.30	1.41	12.6	1.100	87.4	1.941
4	0.60	2.00	16.55	1.218	83.45	1.921
6	0.77	2.44	22.05	1.343	77.5	1.889
8	0.90	2.82	26.65	1.425	73.35	1.865

12	1.07	3.46	30.05	1.477	69.95	1.844
16	1.20	4.00	35.67	1.552	64.33	1.808
20	1.30	4.47	42.43	1.627	57.57	1.760
24	1.38	4.89	46.55	1.667	53.45	1.727

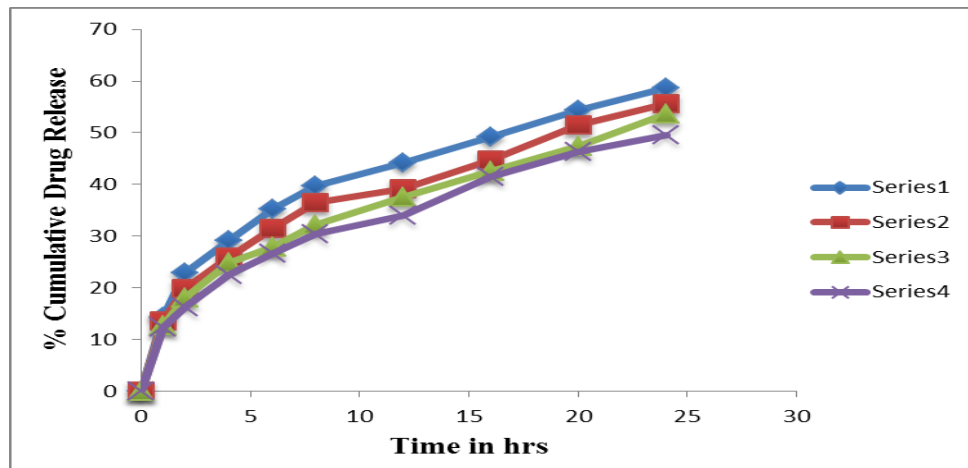


Figure.27: % CDR of nanoemulgel formulation from F2-F5

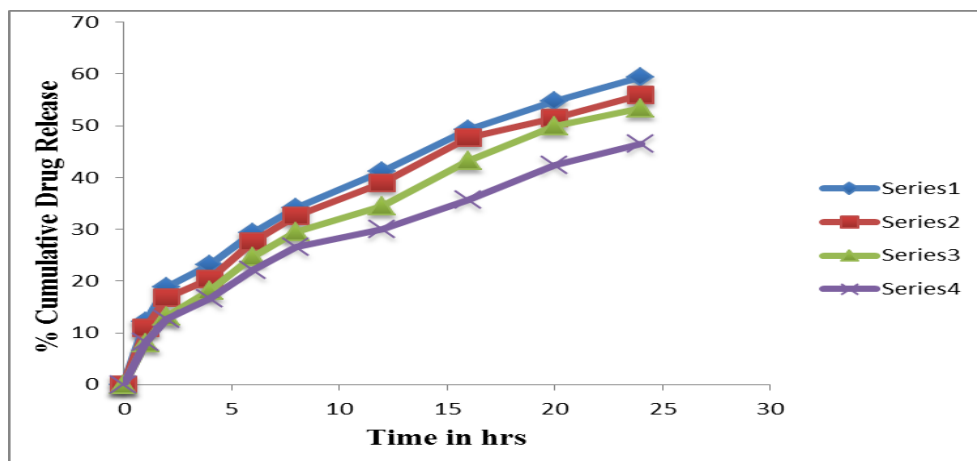


Figure: 28. % CDR of nanoemulgel formulation from F7-F10

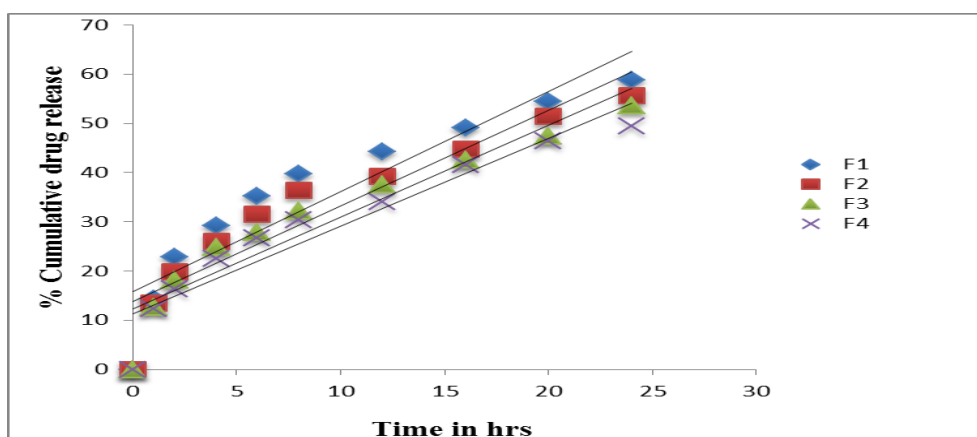


Figure:29. Zero order release kinetic profile of formulation from F2-F5

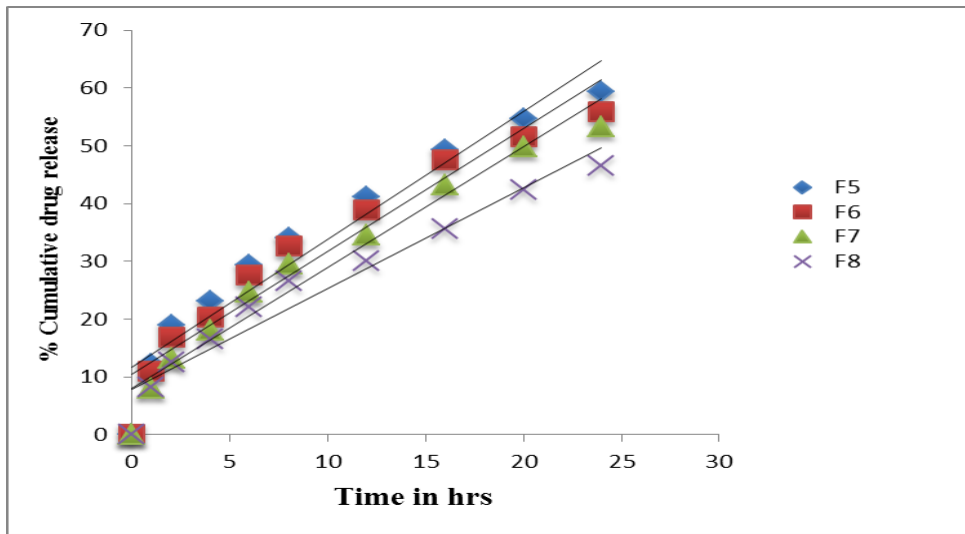


Figure: 30. Zero order release kinetic profile of formulation from F7-F10

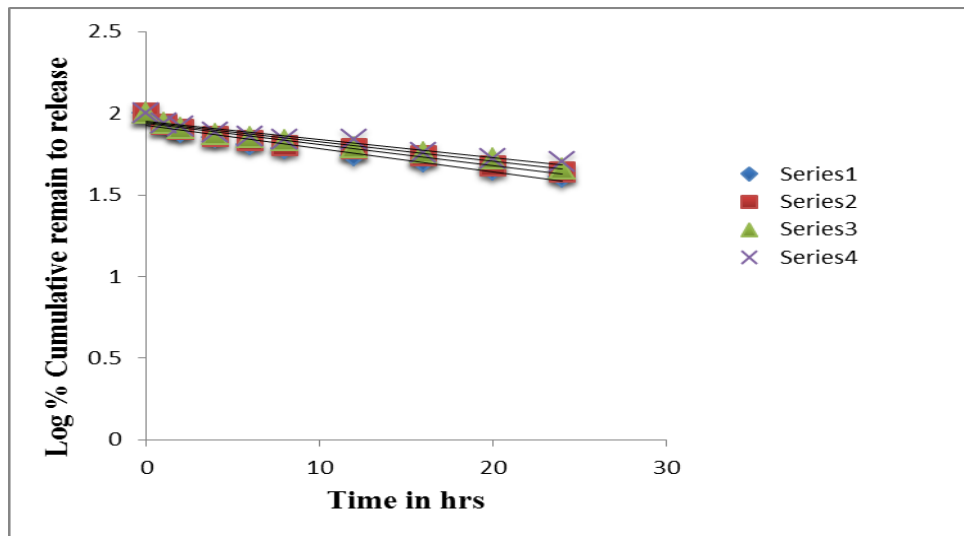


Figure: 31. First order release kinetic profile of formulation from F2-F5

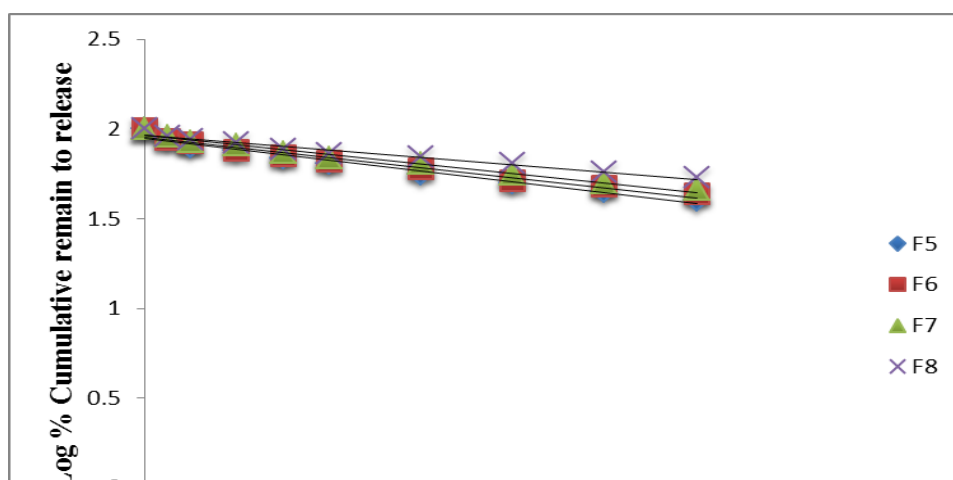


Figure: 32. First order release kinetic profile of formulation from F7-F10

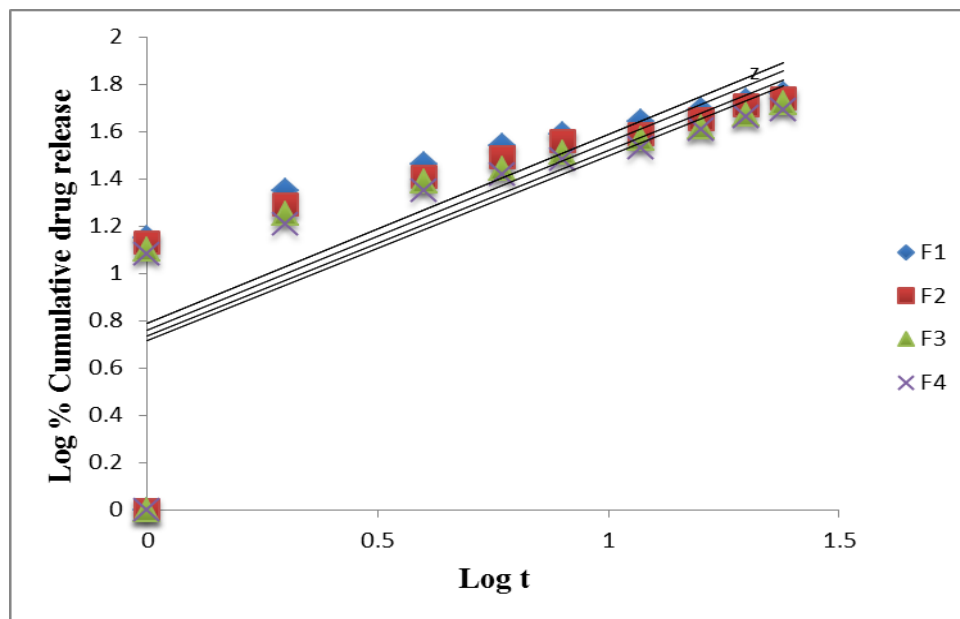


Figure:33. Peppas release kinetic profile of nanosponge formulation from F2-F5

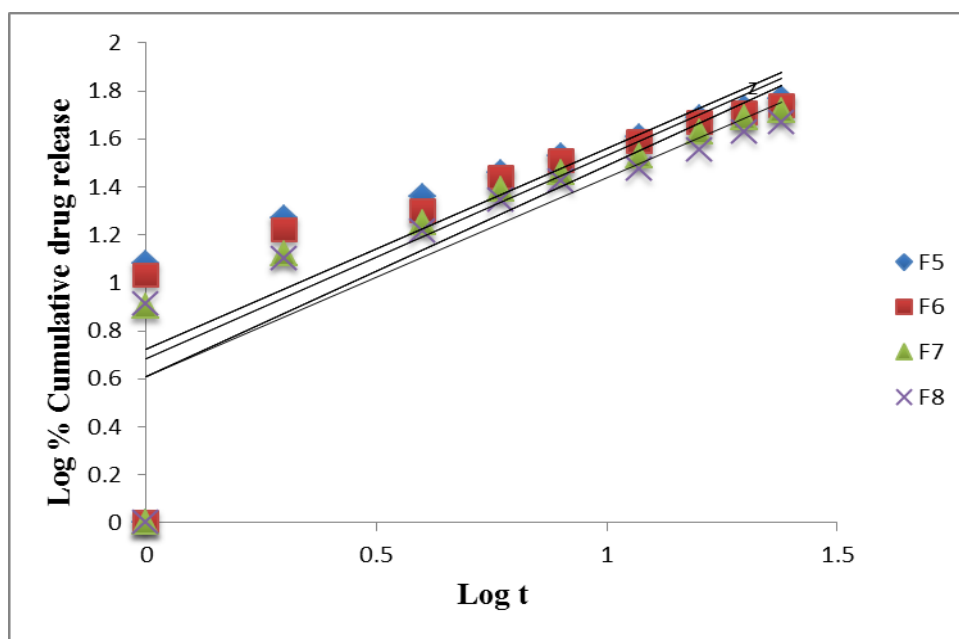


Figure: 34. Peppas release kinetic profile of nanosponge formulation from F7-F10

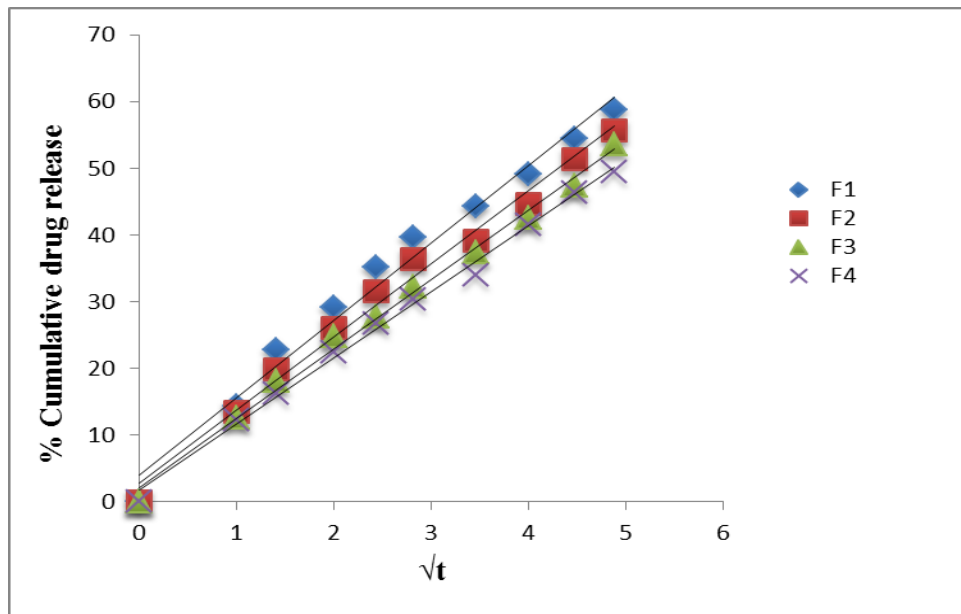


Figure: 35. Higuchi release kinetic profile of nanosponge formulation from F2-F5

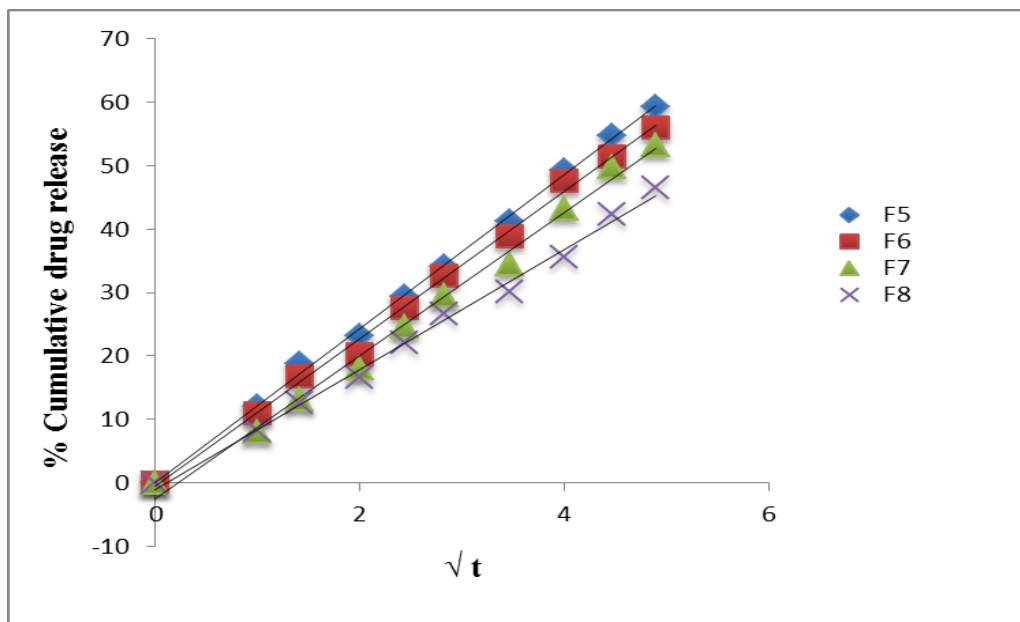


Figure: 36. Higuchi release kinetic profile of nanosponge formulation from F7-F10

Table:24. Comparative *in-vitro* release profile of nanosponge formulation

Formulation code	Zero order	First order	Higuchi plot	Peppas plot	
				r^2	'n'
F2	0.849	0.932	0.983	0.615	0.798
F3	0.876	0.937	0.989	0.630	0.793
F4	0.896	0.946	0.994	0.641	0.785
F5	0.902	0.937	0.995	0.653	0.782
F7	0.927	0.972	0.998	0.678	0.836
F8	0.929	0.966	0.996	0.704	0.845
F9	0.951	0.981	0.993	0.766	0.879
F10	0.942	0.973	0.994	0.744	0.829

4.2.3 Burn wound model



4.2.3.1 Acute skin irritation study

Skin irritation toxicity was conducted in New Zealand White (NZW) Rabbits. On back surface of New Zealand White (NZW) Rabbits, hairs were removed then optimized formulation was applied topically. This study was conducted as per the OECD guidelines for Acute Dermal Irritation in rabbits (OECD 404). Animals were observed once a day for 72 hours after topical application of the formulation. The degrading or score of erythema, eschar, and edema formation was performed as per the below table.

Table:25. Evaluation of skin irritation toxicity

Skin reaction	Observation time	Optimized Formulation I-F4 (Score)	Optimized Formulation II -F10 (Score)
Erythema/Eschar formation	24 h	0	0
	72 h	0	0
Edema formation	24 h	0	0
	72 h	0	0

h- hours; 0-No erythema/edema at all

	Optimized Formulation I (F4)	Optimized Formulation II (F10)
Before application of Formulation		







Application of Formulation		
After 24 H		
After 72 H		

Figure: 37. Skin photographs before and after application up to 72 hrs.

4.2.3.2. Burn wound model in Wistar albino rat

4.2.3.3. Wound contraction

Figure displayed representative images of partial thickness burn wounds in Wistar albino rat. The Table displays the proportion of wound contraction for various treatment groups. Graph-1: Effect of Formulation-1 and 2 on wound area (mm^2) in burn wound model.



Figure: 38. Healing pattern in burn wound model at day 5

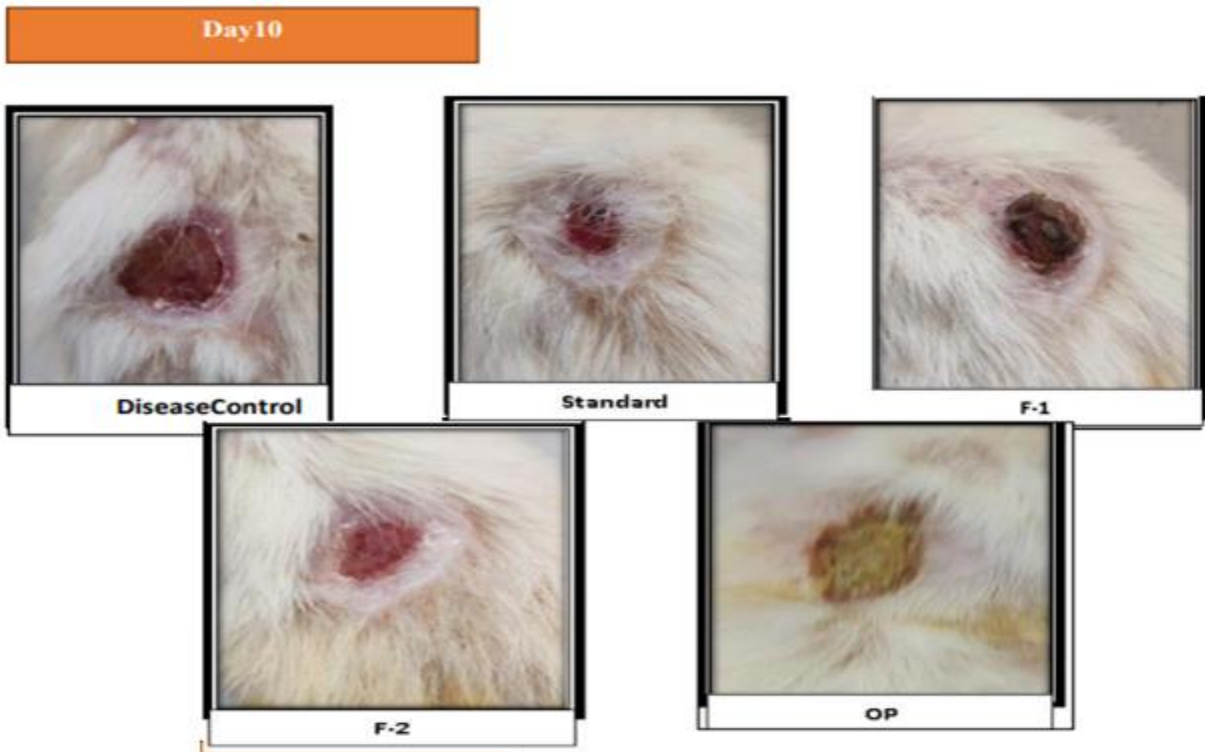


Figure: 39. Healing pattern in burn wound model at day 10

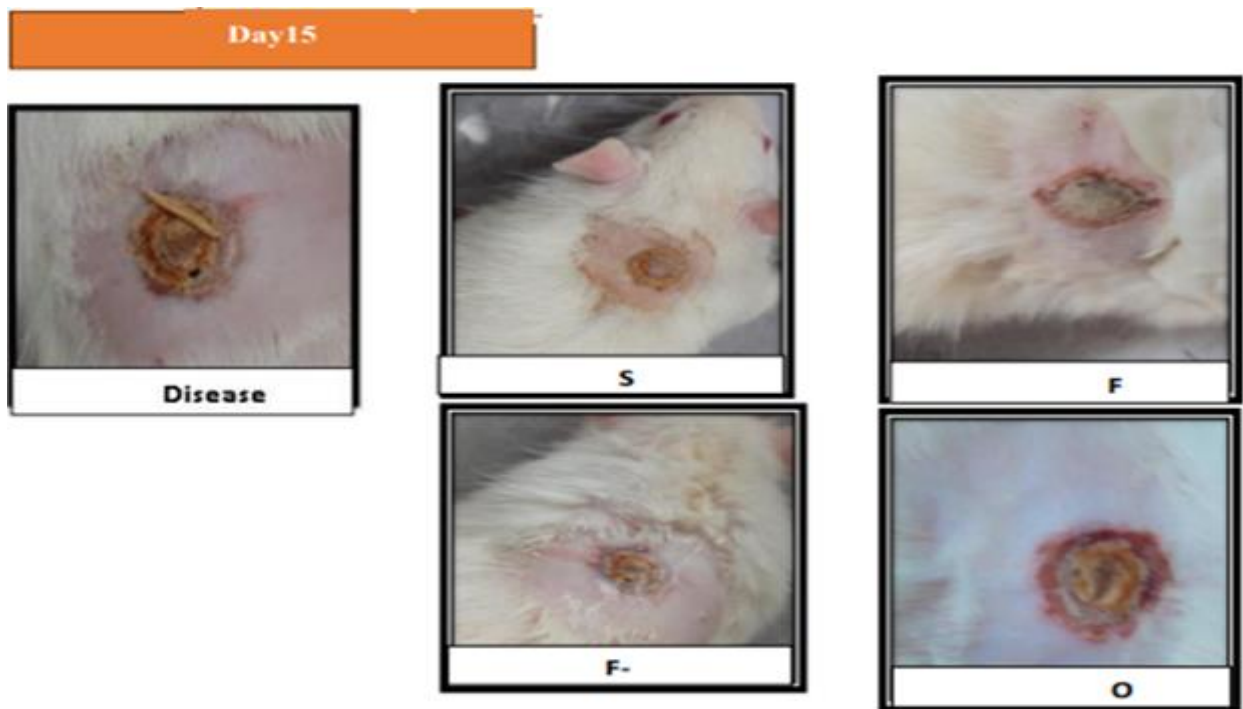


Figure: 40. Healing pattern in burn wound model at day 15

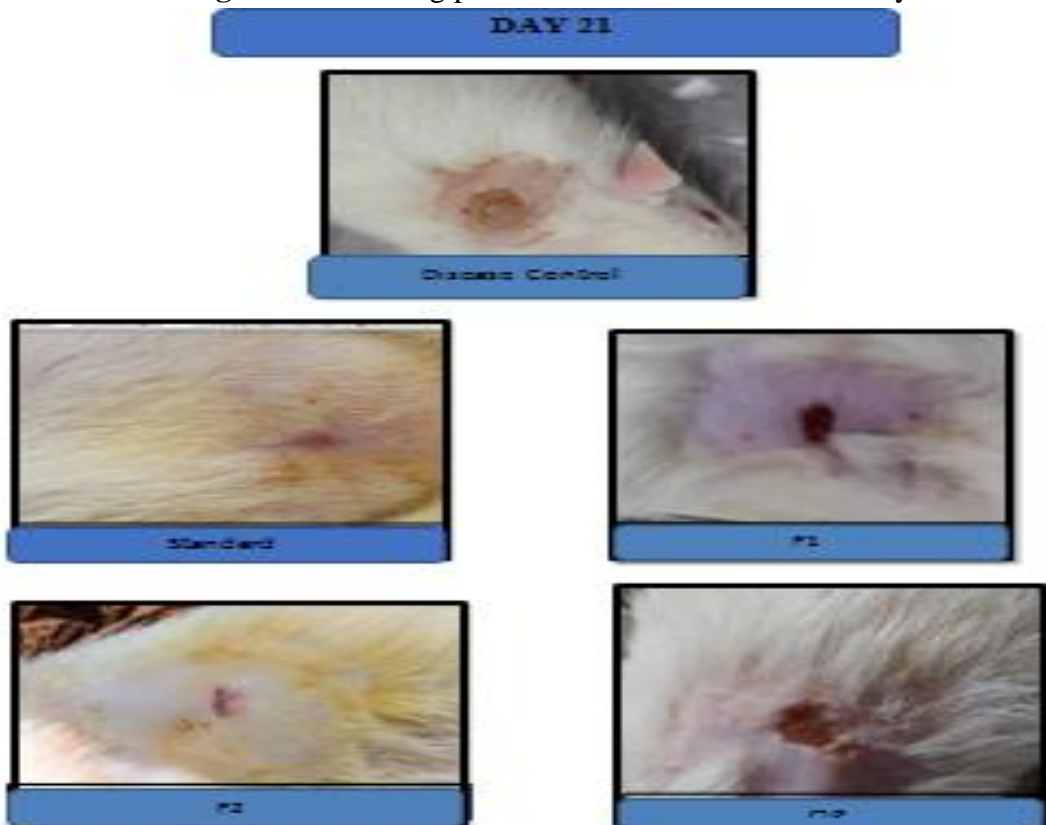


Figure: 41. Healing pattern in burn wound model at day 21

Table:26. Effect of Formulation-1 (optimised formulation F4) and 2 (F10) on % wound contraction in burn wound model

Treatment	0 day	5 days	10 days	15 days	21 days
Control	0	0	0	0	0
NC	0%	14.8%	37.0%	56.5%	75.2%
PC	0%	33.6%	57.5%	73.7%	95.6%
Optimized Formulation-1 (F4)	0%	29.7%	52.5%	68.2%	89.0%
Optimized Formulation-2 (F10)	0%	32.2%	54.3%	70.9%	91.9%
Only Polymer	0%	16.3%	39.6%	61.3%	78.1%

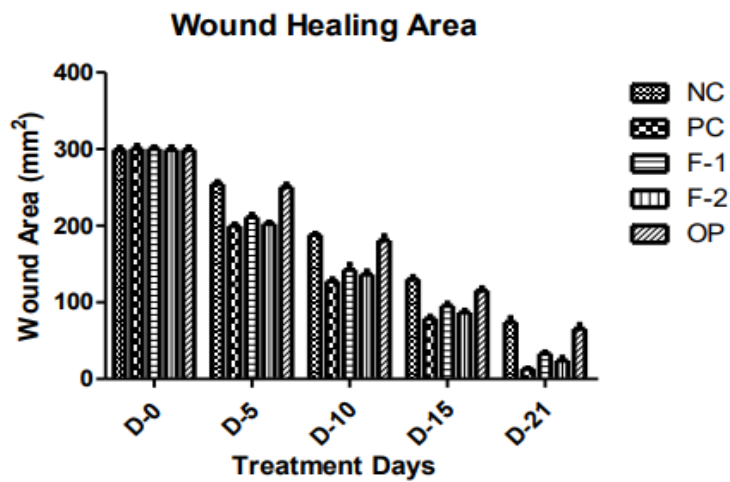


Figure: 42. Effect of optimised formulation on wound area (mm²) in burn wound model

Table:27. Effect of optimised formulation on rate of epithelialization in burn wound model

Treatment	Epithelialization Period (mean \pm SEM)
NC	24.42 \pm 0.40
PC	13.14 \pm 0.79
Formulation-1	18.68 \pm 0.74
Formulation-2	15.4 \pm 0.94
Only Polymer	20.92 \pm 0.81

4.2.3.4 Histopathological observations

The histopathology of several treatment groups is shown in Figure. 4.6.5to 4.6.7. The histological study of the stained samples indicated that the approach used to create burn wounds consistently resulted in the formation of partial thickness burn wounds.

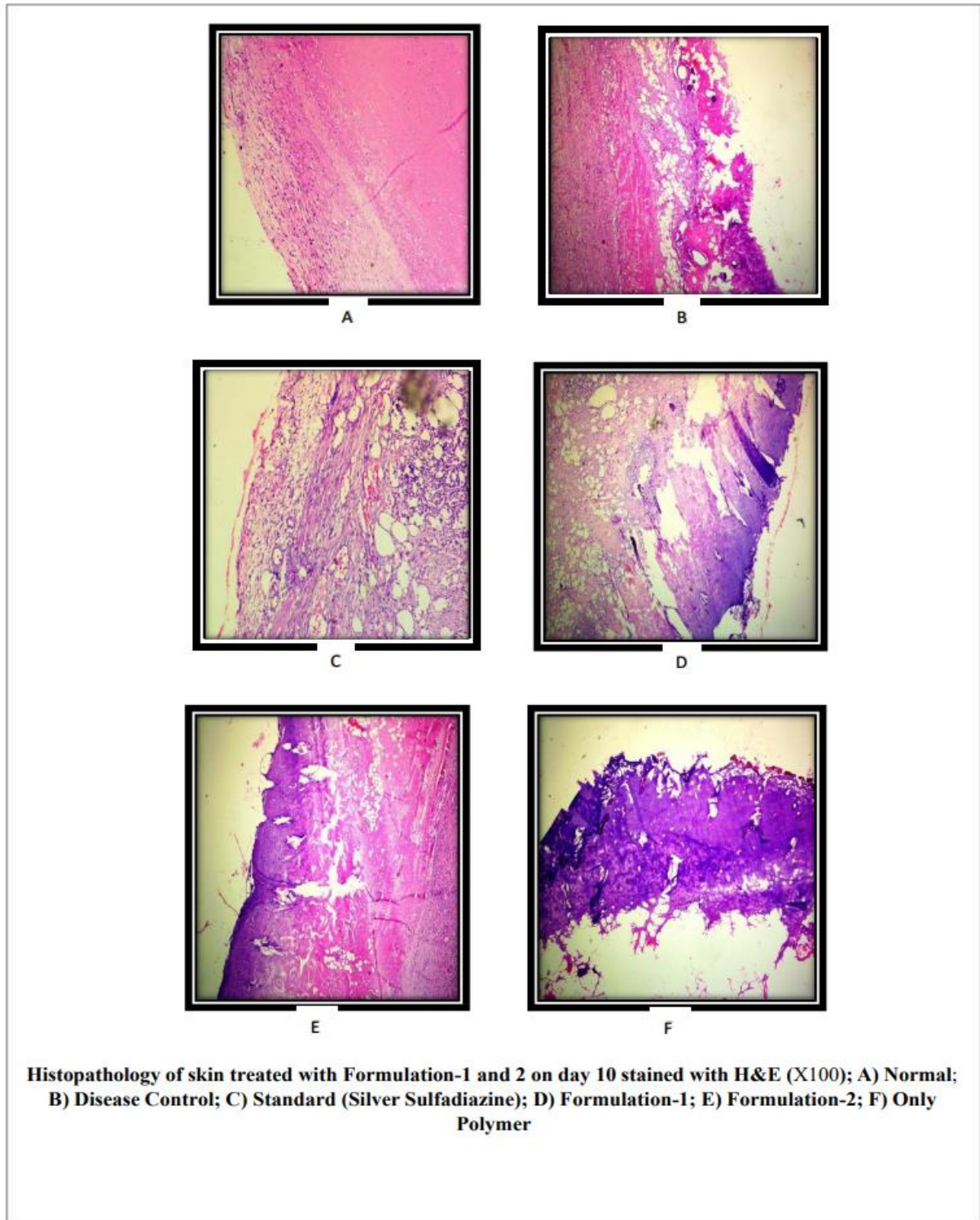


Figure:43. - Histopathological Study on Day 10

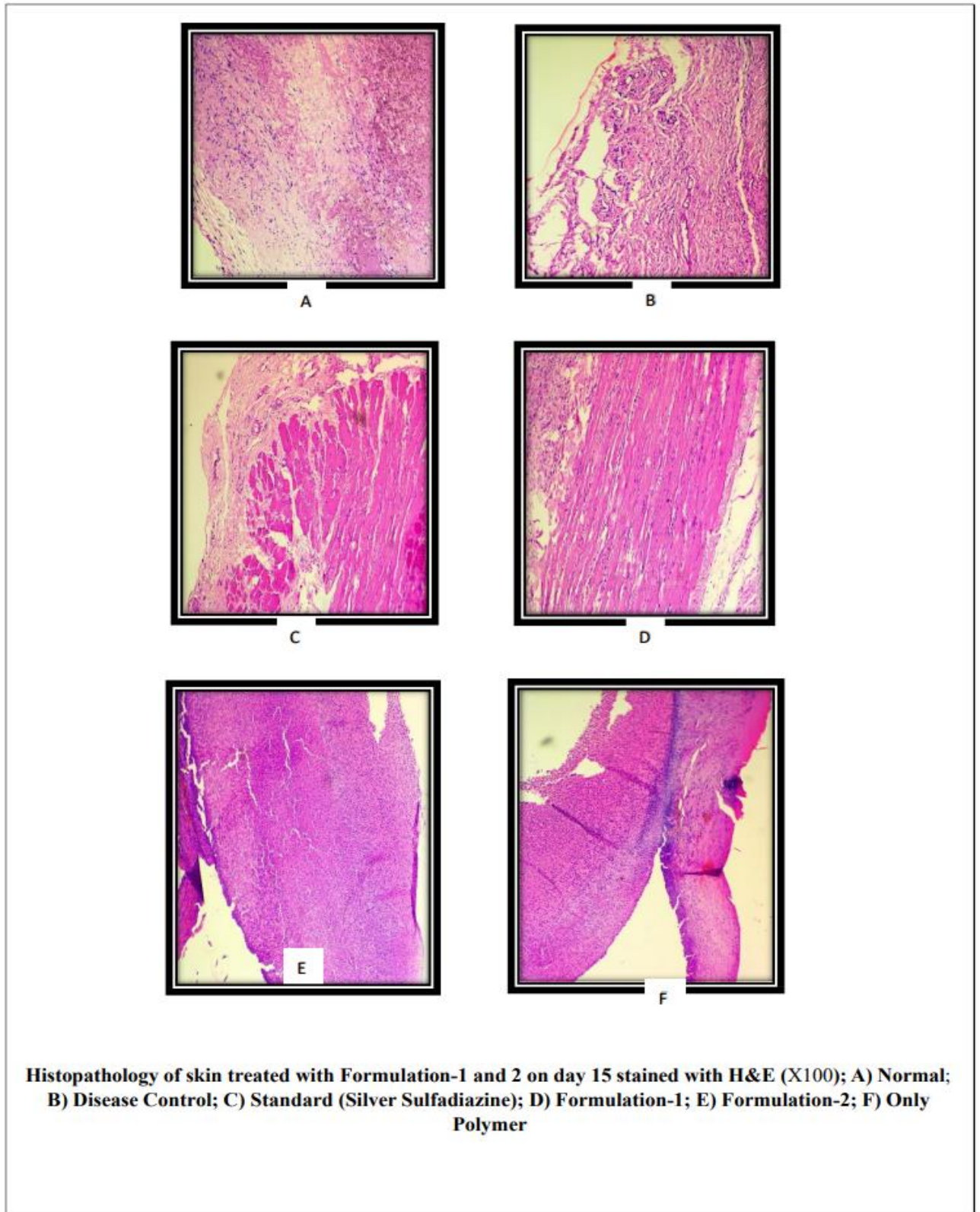
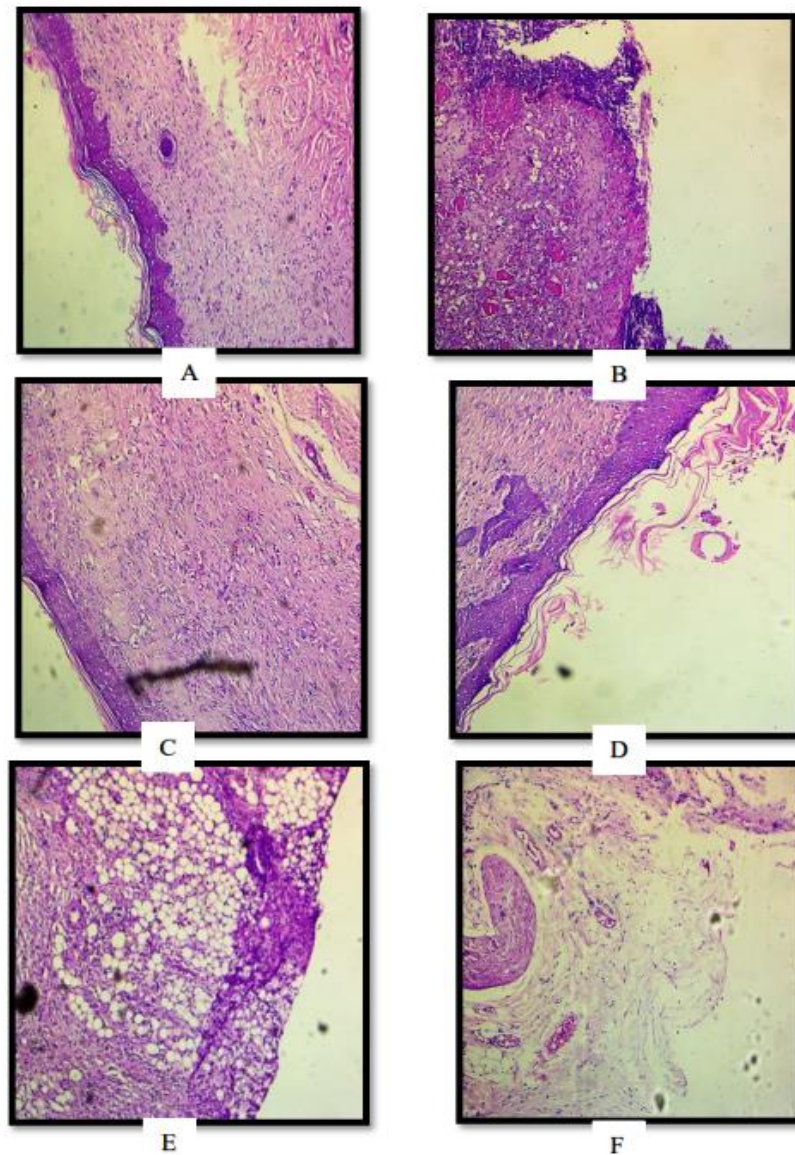


Figure:44. - Histopathological Study on Day 15



Histopathology of skin treated with Formulation-1 and 2 on day 21 stained with H&E (X100); **A) Normal:** normal layers of epidermis and dermis. **B) Disease Control:** Invasive inflammatory cells with no epithelial layer. **C) Standard (Silver Sulfadiazine):** Proper horizontal alignment and interlacement of the dermal fibers, i.e., collagen fibers, are observed. Re-epithelialization is seen almost as normal tissue. The wound site appears more vascular with the presence of hair follicles. **D) Formulation-1:** lack of epithelialization and massive inflammatory cell infiltration. **E) Formulation-2:** partial re-epithelialization and well-formed granulation tissue of epidermis with neovascularization and mild inflammatory cell infiltration. **F) Only Polymer (OP):** inflammatory cell infiltrations along with more collagenation and neovascularization.

Figure:45. - Histopathological Study on Day 21

4.2.3.5 Wound Healing

In the burn-induced wound model, we observed that the wound was healing significantly day-wise in groups 2, 3, and 4 viz. standard treatment, optimised formulation-1 and optimised formulation-2. When compared with standard, optimised formulation-2 groups showed a promising result in wound healing. The wound healing of standard and optimised formulation-2 was best on day-21 i.e. 16 mm² and 24 mm². Table 26 shows % wound contraction day-wise in the burn-induced wound model. When compared to the standard group, optimised formulation 1 and 2 showed better results viz. 95.6% and 91.9% respectively.

The epithelization rate in the burn-induced wound model is depicted in Table 27. The standard shows rate of epithelization 13.14±0.79 and optimised formulation-2 shows 15.4±0.94 which indicates significant results when compared to disease control and only polymer groups.

Overall, optimised formulation is showing promising results in burn-wounded rats and further studies will establish the mechanistic pathways for the same.

4.2.3.6 Hydroxyproline content

Effect on hydroxyproline

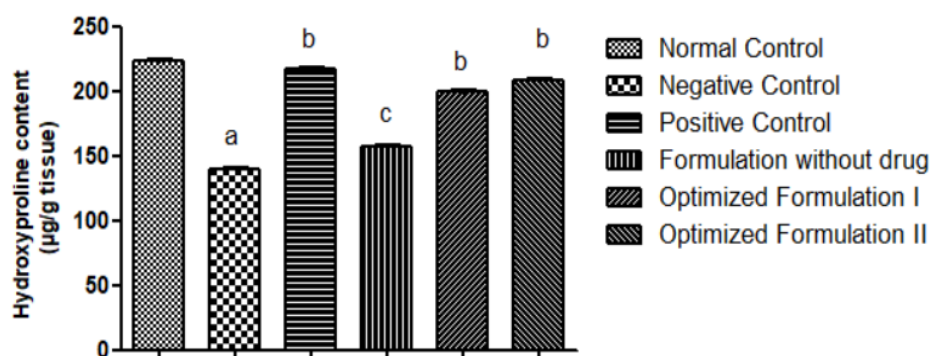


Figure:46. Effect of optimized formulation on hydroxyproline

Results are expressed as mean ± SEM, (n=6); ^aP<0.001 vs normal control group; ^bP<0.001 vs negative control group; ^cP<0.05 vs negative control group.

Hydroxyproline was significantly (P<0.001) reduced in negative control group as compared to normal control group. The hydroxyproline was significantly (P<0.001) elevated in rats treated with optimized formulations and standard drug i.e. silver sulfadiazine, as compared with negative control group.

4.2.3.7 Stability study of optimized formulations: -

Stability Studies: Stability studies of nanosponge to forecast and guarantee shelf life for three acceptance and approval of formulations based on nanosponge in varying temperatures and humidity levels.

There are various types of stability, including toxicological, chemical, physical, microbiological, and therapeutical stability. Stress testing looks at how drugs are affected by changes in humidity, temperature, photolysis, and oxidation. Stress tests also include photostability. Three main batches are included in the selection process; these batches ought

to be produced using the same process used in the final production batch, at the very least on a pilot size. A list of tests, references to analytical techniques, and suggested acceptance criteria are all included in the specification. Testing the characteristics of the drug material that could alter during storage and potentially affect its quality, safety, and/or efficacy is part of stability studies. Testing frequency for drug substances with a minimum 12-month plan for retest intervals, testing frequency for testing for long-term storage conditions should occur every three months during the first year, every six months during the second year, and then once a year for the duration of the suggested re-test period.

Table:28. Accelerated stability studies for optimized formulation of nanosponge based emulgel F4 at $40 \pm 2^\circ\text{C}$ and $75 \pm 5\%$

Parameters	Duration in months			
	0	1	3	6
%Drug content	92.90	92.6	92.2	91.92
pH	6.4	6.45	6.5	6.54
% CDR	49	48.8	48.2	47.3

Table:29. Accelerated stability studies for optimized formulation of nanosponge based emulgel F10 at $40 \pm 2^\circ\text{C}$ and $75 \pm 5\%$

Parameters	Duration in months			
	0	1	3	6
%Drug content	95.26	95.10	95.02	94.42
pH	6.52	6.57	6.59	6.72
% CDR	46.55	46.02	45.82	45.25

Accelerated stability studies were carried out at $40 \pm 2^\circ\text{C}$ and $75 \pm 5\%$ RH for the optimized formulation F4 and F10 monitored for drug content, pH and dissolution profile study. The results are shown in table 29, 30 which indicated that all the nanosponge based emulgel were stable during storage period.

5. CONCLUSION

Preformulation studies of Silver sulphadiazine were carried out by determination Melting point, solubility, and λ_{max} . The obtained results complied with IP standards thus indicating the purity of drug. The drug-excipients compatibility by FT-IR and DSC confirmed no significant interaction between drug and selected excipients. The average particle size was found to be in the nm range and showed ideal surface morphology. The zeta potential of selected formulation F4 and F10 were found to be -53.4 mV and -36.6 mV which indicate that the formulations are stable. F4 and F10 formulation taken as optimized formulation because of high drug content, high entrapment efficiency and better controlled release compare to other formulation and these two formulations was taken for stability studies and preparation of gel.

In-vitro drug release study confirmed that the Silver sulphadiazine nanosponge based emulgel formulation F4 and F10 has better potential of control drug release. Overall the curve fitting in to various kinetic models confirmed that the *in-vitro* releases of all the formulations were best fitted in to Higuchi model followed by Peppas plot. The 'n' values more than 0.5 indicates that the mechanism in which the drug release from nanosponge follows Non-Fickian diffusion-controlled system. Skin irritation study shows that prepared nanosponge based emulgel formulation are compatible with no skin irritation to animal skin and can be used for further studies.

In the burn-induced wound model results are showing that the wound was healing significantly day-wise in groups 2, 3, and 4 viz. standard treatment, optimised formulation-4 and optimised formulation-10. When compared with standard, optimised formulation-2 groups showed a promising result in wound healing. The wound healing of standard and optimised formulation-4 was best on day-21 i.e. 16 mm² and 24 mm². When compared to the standard group, optimised formulation showing wound contraction results viz. 95.6% and 91.9% respectively. The epithelization rate in the burn-induced wound model is depicted and standard shows rate of epithelization 13.14±0.79 and optimised formulation-2 shows 15.4±0.94 which indicates significant results when compared to disease control and only polymer groups. Overall, optimised formulation is showing promising results in burn-wounded rats and further studies will establish the mechanistic pathways for the same.

Stability studies of selected formulation F4 and F10 showed that, negligible changes in drug content, pH and % CDR and revealed that the formulations are stable on storage. The research concludes that the SSD-loaded nanosponge emulgel formulation exhibits significant potential as a topical delivery system for wound healing. Key findings include:

The emulgel formulation provided a stable medium for the SSD-loaded nanosponges, preventing aggregation and ensuring a uniform distribution of the active agent.

The nanosponge structure facilitated a sustained release of silver sulphadiazine, maintaining therapeutic levels over an extended period. *In-vitro* and *In-vivo* studies demonstrated superior antimicrobial activity and enhanced wound healing compared to conventional SSD formulations.

The study supports the potential of nanosponge-based emulgel as an effective and innovative approach for topical wound healing applications. Further clinical trials and long-term studies are recommended to validate these findings and explore the full therapeutic potential of this novel formulation.

CONFLICT OF INTEREST: None

DECLARATION: None

ACKNOWLEDGEMENT

Author would like to express gratitude to Faculty of Pharmacy, Swami Vivekanand Subharti University, Meerut and Bharat Institute of technology, Meerut for their support during work. I am thank full to Dr. Neeta, Associate Professor, Department of Pharmaceutical Sciences, Maharshi Dayanand University, Rohtak & Mrs. Priyanka Singh, Department of Pharmacy, Banasthali University, Rajasthan, Dr. Ravinder Kumar Mehra from Bharat Institute of Technology, Meerut, Dr. Dinesh Kumar from Desh Bhagat University, Mandi Gobindgarh and Dr. Shardendu Mishra from Krishna Institute of Engineering and Technology, Ghaziabad for their help throughout the course of study for their continuous support.

REFERENCES:

1. Oncul O, Yuksel F, Altunay H, Acikel C, Celikoz B, Cavuslu S. The evaluation of nosocomial infection during 1-year-period in the burn unit of a training hospital in Istanbul, Turkey. *Burns* 2002; 8:738-44
2. Taneja N, Chari P, Singh M, Singh G, Biswal M, Sharma M. Evolution of bacterial flora in burn wounds: key role of environmental disinfection in control of infection. *Int. J. Burns Trauma*. 2013; 2:102-7.
3. Wertheim HF, Verveer J, Boelens HA, van Belkum A, Verbrugh HA, Vos MC. Effect of mupirocin treatment on nasal, pharyngeal, and perineal carriage of *Staphylococcus aureus* in healthy adults. *Anti microb. Agents Chemother*. 2005; 4:1465
4. Williams RE. Healthy carriage of *Staphylococcus aureus*: its prevalence and importance. *Bacteriol.Rev*. 1963:56-71.
5. Jackson DM. The diagnosis of the depth of burning. *Br.J.Surg*. 1953;164:588-96.
6. Jodar KS, Balcao VM, Chaud MV, Tubino M, Yoshida VM, Oliveira Jr JM, Vila MM. Development and characterization of a hydrogel containing silver sulfadiazine for antimicrobial topical applications. *Journal of Pharmaceutical Sciences*. 2015;104(7):2241- 2254.
7. Kong HH. Skin microbiome: genomics-based insights into the diversity and role of skin microbes. *Trends Mol.Med*. 2011;6:320-8.
8. Cakir B, Tegen B. Systemic Responses to Burn Injury. *Turkish Journal of Medical Sciences* 2004:215-262
9. Chiller K, Selkin BA, Murakawa GJ. Skin microflora and bacterial infections of the skin. *J.Investig.Dermatol.Symp.Proc*. 2001;3:170-4.
10. Chhabra S, Chhabra N, Kaur A, Gupta N. Wound healing concepts in clinical practice of OMFS. *J Maxillofac Oral Surg*. 2017;16(04):403–423.
11. Evans CA, Smith WM, Johnston EA, Giblett ER. Bacterial flora of the normal human skin. *J. Invest. Dermatol*. 1950; 4:305-24.
12. Murthy S, Gautam MK, Goel S, Purohit V, Sharma H, Goel RK. Evaluation of in vivo wound healing activity of *Bacopamonniera* on different wound model in rats. *Biomed Res Int*. 2013; 2013:972028. doi: 10.1155/2013/972028.
13. Newman RE, LoganMA.The determination of hydroxyproline.The Journal of

- Biological Chemistry, 1950; 184(1):299–306.
14. .R. Gangadhara*, K. P. Satheesh1, N. Devanna, L. Sasikala and Vandavasi Koteswara Rao. Formulation and invitro characterization of ketorolac loaded nanosponges, international journal of research in pharmacy and chemistry.,IJRPC 2021, 11(3), 99-103
 15. Al Laham NA, Elmanama AA, Tayh GA. Possible risk factors associated with burn wound colonization in burn units of Gaza strip hospitals, Palestine. Ann. Burns Fire Disasters. 2013; 2, 68-75.
 16. Kushwaha, A, Goswami, L, Kim, B.S. Nanomaterial-Based Therapy for Wound Healing. Nanomaterials 2022, 12, 618. [https:// doi.org/10.3390/nano12040618](https://doi.org/10.3390/nano12040618).
 17. Karam F. Abdalla a, Mohamed A. Osman a, Ahmed T. Nouh b, Gamal M. El Maghraby a. Microsponges for controlled release and enhanced oral bioavailability of carbamazepine. Journal of Drug Delivery Science and Technology. (2021); 65:102683
 18. Kaur T, Kapoor DN. Development and evaluation of sea buckthorn (*Hippophae rhamnoides* L.) seed oil nanoemulsion gel for wound healing. Pharmacognosy Magazine. 2018;14(58):647-658
 19. Muller MJ, Hollyoak MA, Moaveni Z, Brown TL, Herndon DN, Heggers JP. Retardation of wound healing by silver sulfadiazine is reversed by Aloe vera and nystatin. Burns. 2003;29(8):834-836.
 20. Sandri G, Bonferoni MC, D’Autilia F, Rossi S, Ferrari F, Grisoli P, Sorrenti M, Catenacci L, Del Fante C, Perotti C, Caramella C. Wound dressings based on silver sulfadiazine solid lipid nanoparticles for tissue repairing. European Journal of Pharmaceutics and Biopharmaceutics. 2013;84(1):84-90.
 21. Sharma R, Kumar R, Mittal S, Kaur A. Study of effect of topical nano silver gel on wound healing. Journal of Advanced Medical and Dental Sciences Research. 2016;4(5):59- 61.
 22. Sharma R, Pathak K. Polymeric nanosponges as an alternative carrier for improved retention of econazole nitrate onto the skin through topical hydrogel formulation. Pharmaceutical Development and Technology. 2011;16(4):367-376.
 23. Shanuja J, Kajal Singh, Sai Nandhini, Jayanthi Palanivelu, (2021). Nanosponges: In Perspective to Therapeutic Medicine. In: Arivarasan, V.K., Loganathan, K., Janarthanan, P. (eds) Nanotechnology in Medicine. Nanotechnology in the Life Sciences. Springer, Cham. https://doi.org/10.1007/978-3-030-61021-0_6
 24. Venkataraman M, Nagarsenker M. Silver sulfadiazine nanosystem for burn therapy. AAPS Pharm SciTech. 2013;14(1):254-264.
 25. Yu M, Ma H, Lei M, Li N, Tan F. *In-vitro/in-vivo* characterization of nanoemulsion formulation of metronidazole with improved skin targeting and anti-rosacea properties. European Journal of Pharmaceutics and Biopharmaceutics. 2014;88(1):92-103.
 26. Yadav GV, Panchory HP. Nanosponges—a boon to the targeted drug delivery system. J Drug Delivery Ther 2013; 3:151-5.